UNIVERSITÀ DEGLI STUDI DI PADOVA

DIPARTIMENTO DI SCIENZE CHIRURGICHE, ONCOLOGICHE E GASTROENTEROLOGICHE

SCUOLA DI DOTTORATO DI RICERCA IN ONCOLOGIA E ONCOLOGIA CHIRURGICA

CICLO XXV

TESI DI DOTTORATO

COLON STEM CELL CHARACTERIZATION IN NORMAL AND TUMORAL TISSUES: DESCRIPTION OF A NOVEL FEED-FORWARD CIRCUIT OF MSI-1 REGULATION

Direttore della Scuola: Ch.ma Prof.ssa Paola Zanovello

Supervisore: Prof. Alberto Amadori

DOTTORANDA: Dott.ssa Anna Pastò

INDEX

ABSTRACT

Normal tissues are organized in a hierarchical fashion, where rare somatic cells endowed with stem-like properties give origin to a population of differentiated cells forming the bulk of tissue. These self-maintaining cells, called stem cells, are characterized by 4 fundamental properties: longevity, multipotency, quiescence, and asymmetric cell division.

We decided to develop a new *in vitro* system for separation of stem-like epithelial cell based not on surface marker-driven selection, but by simply taking advantage of their slow proliferation rate in the absence of serum.

Dissociated colonic epithelial cells were stained with PKH26, which allows identification of distinct populations based on their proliferation rate, and cultured *in vitro* in the absence of serum. The cytofluorimetric expression of CK20, Msi-1 and Lgr5 was studied. The mRNA levels of several stemness-associated genes were also compared in cultured cell populations and in three colon crypt populations isolated by microdissection. A PKH^{pos} population survived in culture and formed spheroids; this population included subsets with slow (PKH^{high}) and rapid (PKH^{low}) replicative rates. Molecular analysis revealed higher mRNA levels of both Msi-1 and Lgr5 in PKH^{high} cells; by cytofluorimetric analysis, $Msi\text{-}1^{+}/Lgr5^{+}$ cells were only found within PKH^{high} cells, whereas $Msi\text{-}1^{+}/Lgr5^{-}$ cells were also observed in the PKH^{low} population. As judged by qRT-PCR analysis, the expression of several stemness-associated markers (Bmi-1, EphB2, EpCAM, ALDH1) was highly enriched in $Msi\text{-}1^{+}/Lgr5^{+}$ cells. While CK20 expression was mainly found in PKH^{low} and PKH^{neg} cells, a small PKH^{high} subset co-expressed both CK20 and Msi-1, but not Lgr5; cells with these properties also expressed Mucin-1, and could be identified *in vivo* in colon crypts. These results mirrored those found in cells isolated from different crypt portions by microdissection, and based on proliferation rates and marker expression they allowed to define a hierarchy of cellular subsets at different maturation stages: $PKH^{high}/Lgr5^{+}/Msi\text{-}1^{+}/CK20^{-}$, $PKH^{high}/Lgr5^{-}/Msi\text{-}1^{+}/CK20^{+}$, $PKH^{low}/Lgr5^{-}/Msi\text{-}1^{+}/Ck20^{-}$, and $PKH^{low}/ Lgr5^{-}/Msi\text{-}1^{-}/ CK20^{+}$ cells.

We next addressed the issue of cancer stem cells in colorectal cancer (CRC). Isolated cells from five primary colon tumors and 15 CRC metastatic samples were stained with PKH26 and cultured in PhEMA-treated plate in the absence of serum.

As in normal samples, in tumors we identified a slowly cycling population able to persist in vitro in serum-free condition. On the contrary, in metastatic samples we could not document an *in vitro* selection of a PKH^{high} population; actually PKH^{low} cells seemed to remain constant over several weeks. Cytofluorimetric analysis revealed that, at variance with normal samples, in metastatic samples $Lgr5^{+}$/$Msi\text{-}1^{+}$ cells were not only present in the slowly cycling PKH^{high} population but also in PKH^{low} cells. No Lgr5 or Msi-1 expression was recorded in PKH^{neg} cells. Both PKH^{high} and PKH^{low} cells were able to form spheroids; in the presence of 10% FCS in uncoated plates they adhered to the plate and differentiated assuming an epithelial morphology. They eventually lost Msi-1 and Lgr5 expression after 14 days of culture in the presence of serum and adhesion conditions, and they also acquired CK20 expression.

Finally, we investigated the possible involvement of Notch signaling on regulation of Msi-1 levels in the metastatic cell line $MICOL\text{-}14^{tum}$ and primary metastatic samples. Seventy two hours of treatment with the Notch ligand DLL4 increased Msi-1 mRNA and protein levels. This phenomenon was largely prevented by the addition of an antibody neutralizing Notch2/3, whereas no reduction was detected after incubation with α-Notch1. Since Msi-1 regulates Numb levels, its reduction led to increased Numb protein, as demonstrated by Western Blot analysis of $MICOL\text{-}14^{tum}$ and primary metastatic cells. Furthermore, after four days of treatment, formation of spheroids was significantly reduced by incubation with α-Notch2/3 antibody in primary samples as well as in $MICOL\text{-}14^{tum}$ cells.

In conclusion, our data showed the possibility of deriving *in vitro* from normal colon tissue, without any selection strategy, an array of cellular subsets differentially expressing the most common stemness and differentiation markers of human colon epithelial cells, which recapitulate the phenotypic and molecular profile of cells in an anatomical position compatible with stem-like cells.

Furthermore in metastatic cell line and primary samples we described a novel feed-forward circuit involving Msi-1, Numb, Notch3 and Notch1. In particular, we demonstrated that Msi-1 could be considered a target of Notch3, and Notch3 could act as a positive regulator of Notch1 levels through Msi-1/Numb circuit.

RIASSUNTO

I tessuti normali non patologici sono organizzati in una struttura gerarchica all'interno della quale un numero esiguo di cellule origina l'intera totalità della popolazione. Queste cellule presentano longevità, multipotenza, quiescenza e capacità di dividersi in maniera asimmetrica, tutte caratteristiche di staminalità.

Abbiamo deciso di sviluppare un sistema *in vitro* per separare le cellule staminali epiteliali del colon, non basandoci sull'espressione di specifici marcatori di superficie, ma semplicemente traendo vantaggio dal ridotto tasso di proliferazione che queste cellule presentano quando tenute in assenza di siero.

Da campioni primari di colon le cellule epiteliali sono state dissociate, marcate con PKH26, che permette l'identificazione di distinte sottopopolazioni basandosi sul tasso di proliferazione, e coltivate *in vitro* in assenza di siero. Sono stati analizzati i livelli di espressione proteica di CK20, Msi-1 e Lgr5 e di mRNA di alcuni geni associati alla staminalità. L'espressione di questi geni è stata confrontata tra la popolazione cellulare in cultura e tre sottopopolazioni isolate dalle cripte di colon attraverso microdissezione laser.

In coltura abbiamo identificato una popolazione PKH^{pos}, in grado di sopravvivere e formare sferoidi, comprendente cellule con un ridotto tasso di proliferazione (PKH^{high}) e cellule con rapido tasso (PKH^{low}). L'analisi citofluorimetrica ha dimostrato che cellule $Msi\text{-}1^{+}/Lgr5^{+}$ si trovano solo nella popolazione PKH^{high}, mentre cellule $Msi\text{-}1^{+}/Lgr5^{-}$ sono presenti anche nella popolazione PKH^{low}. Questi risultati sono stati supportati dall'analisi molecolare nelle diverse sottopopolazioni. Nelle cellule $Msi\text{-}1^{+}/Lgr5^{+}$ abbiamo, infatti, riscontrato livelli più alti di espressione di geni associati con la staminalità (Bmi-1, EphB2, EpCAM, ALDH1). Invece l'espressione di citocheratina (CK20) è quasi totalmente ristretta alle cellule PKH^{low} e PKH^{neg}, le quali esprimono anche Mucin-1 ma non Lgr5.

Questi risultati rispecchiano quelli trovati analizzando le popolazioni isolate dalle diverse porzioni delle cripte attraverso microdissezione, e ci hanno permesso di definire una gerarchia di sottopopolazioni cellulari diverse in differenti fasi di maturazione: $PKH^{high}/Lgr5^{+}/Msi\text{-}1^{+}/CK20^{-}$, $PKH^{high}/Lgr5^{-}/Msi\text{-}1^{+}/CK20^{+}$, $PKH^{low}/Lgr5^{-}/Msi\text{-}1^{+}/Ck20^{-}$, e $PKH^{low}/ Lgr5^{-}/Msi\text{-}1^{-}/ CK20^{+}$.

Per valutare la presenza di diverse sottopopolazioni con caratteristiche di staminalità anche nel tessuto tumorale, da 5 campioni di tumore primario colorettale e da 15 di metastasi, abbiamo isolato le cellule, marcate con PKH26 e mantenute in assenza di siero. Come per i campioni normali, nei tumori abbiamo identificato una popolazione cellulare poco proliferante e in grado di sopravvivere in vitro in assenza di siero. Invece, nei campioni metastatici non siamo stati in grado di definire chiaramente una popolazione PKH^{high}; sembra, infatti, che siano le cellule PKH^{low} in grado di sopravvivere più a lungo in cultura e quindi selezionarsi.

L'analisi citofluorimetrica ha dimostrato che, a differenza dei campioni normali, in quelli metastatici cellule $Lgr5^{+}$/$Msi\text{-}1^{+}$ non sono presenti solo nella popolazione PKH^{high}, ma anche all'interno della sottopopolazione PKH^{low}. Nelle cellule PKH^{neg} invece non si riscontra l'espressione nè di Lgr5 nè di Msi-1. Entrambe le popolazioni PKH^{high} e PKH^{low} sono state in grado di formare sferoidi e, quando mantenute in presenza del 10% di siero, hanno aderito alle piastre differenziandosi ed assumendo una morfologia epiteliale. Queste cellule perdono conseguentemente l'espressione di Msi-1 e Lgr5 solo dopo 14 giorni in queste condizioni, mentre acquistano l'espressione di CK20.

Vista la ridotta presenza di dati inerenti la regolazione di Msi-1, abbiamo infine indagato il possibile coinvolgimento del pathway di Notch sulla regolazione di Msi-1 nelle cellule di tumore del coloretto. Dopo 72 ore di trattamento con il ligando di Notch (DLL4) i livelli di proteina e mRNA di Msi-1 aumentano. Questo fenomeno è bloccato dall'aggiunta di un anticorpo neutralizzante Notch2/3, mentre nessuna variazione è stata riscontrata dopo il trattamento con α-Notch1. Poiché Msi-1 regola i livelli di Numb, la sua diminuzione comporta un aumento dei livelli proteici di Numb, come riscontrato dall'analisi Western Blot effettuata nei campioni tumorali primari e nella linea cellulare $MICOL\text{-}14^{tum}$. Inoltre, dopo quattro giorni di trattamento, la formazione di sferoidi appare significativamente ridotta dal trattamento con α-Notch2/3.

In conclusione, i nostri dati dimostrano la possibilità di derivare *in vitro* da campioni di colon normale, senza alcuna strategia selettiva, delle sottopopolazioni in differenti fasi di maturazione. Inoltre, nel tessuto metastatico siamo stati in grado di descrivere un possibile circuito di regolazione che coinvolge Msi-1, Numb, Notch3 e Notch1. In particolare, abbiamo dimostrato che Msi-1 può esser considerato un target

di Notch3, e Notch3 può agire come un regolatore positivo di Notch1 attraverso il circuito Msi-1/Numb.

INTRODUCTION

1. NORMAL STEM CELLS

1.1 Features

Stem cells (SC) are undifferentiated cells destined to replenish the pool of mature cells whenever needed; for instance, they start to differentiate in response to specific stimuli such as injury. Based on their ability to differentiate, SC are classified as **totipotent** (cells able to give rise to a new individual i.e. embryonic SC), **pluripotent** (cells able to give rise to almost all tissues of the body), or **multipotent** (cells able to generate more cell types on a certain location or single histotype) [1]. In the last group we enclose adult SC, whose main function is tissue homeostasis and repair after injury [2]. Adult SC are cells characterized by three distinct properties:

1) prolonged lifespan

2) ability to self-renewal

3) potential to generate all the differentiated populations within the tissue in which they reside.

Besides longevity and multipotency, another feature commonly attributed to stem cells is a relative quiescence. In fact, although residing in most rapidly renewing tissues such as intestine or stomach, SC are supposed to divide infrequently, and, when they do not divide, they are able to enter in a quiescent state (G_0) of the cell cycle [3]. At variance with non-SC, when proliferating, SC can undergo asymmetric division, eventually producing one rapidly cycling cell and another that replaces the parental stem cell. The rapidly cycling daughter cells, also called *transit-amplifying* cells (TA), are responsible for replacing damaged or exfoliated tissues. TA cells typically undergo a limited number of cell divisions, after which they terminally differentiate.

As depicted in Figure 1, adult SC can potentially follow 3 models of cell division: symmetric division to generate two cells with stem phenotype, asymmetric division giving rise to two types of cells (daughter cell with the same stem properties and dividing potential, and a progenitor TA cell which has limited proliferation potential) or symmetric division to generate two daughter TA cells.

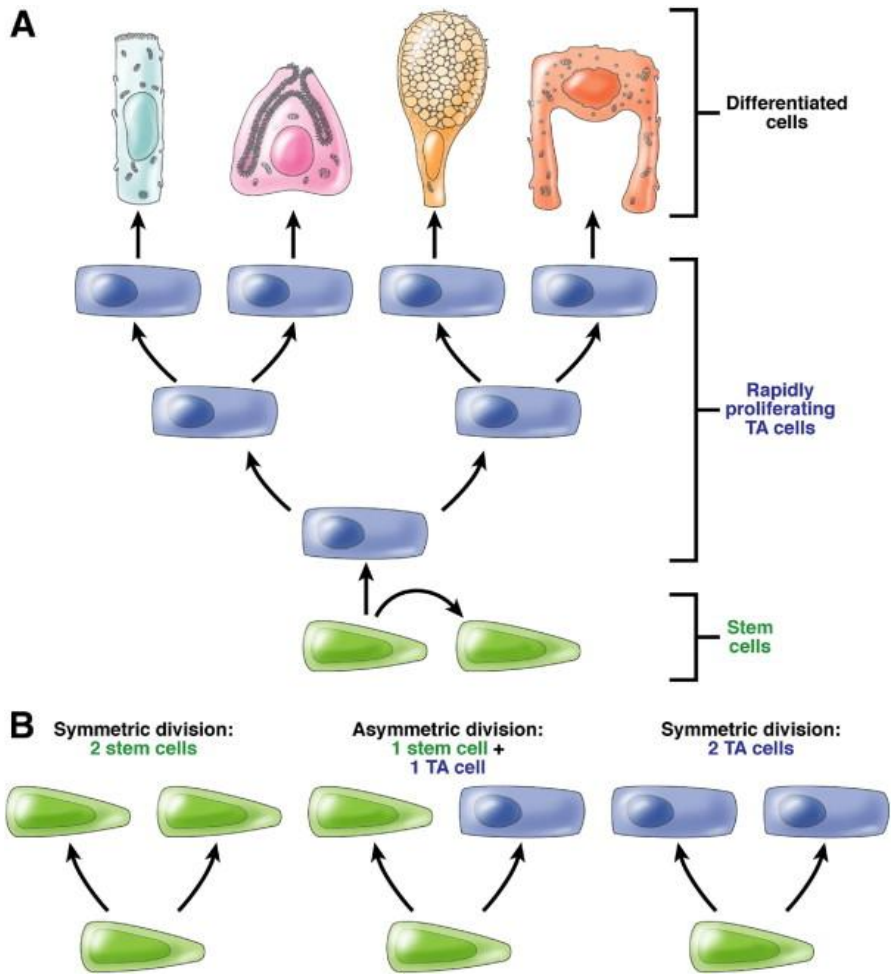

Figure1. **Adult SC–driven tissue-renewal in colon**. (*A*) Stem cells concomitantly self-renew and generate rapidly dividing TA daughter cells via asymmetric cell division. The TA cells undergo several rounds of division before differentiating into the mature, functional cell types of the adult tissue; (*B*) Three models of cell division: two symmetric and one asymmetric division [4].

In adults, SC reside in a physiologically limited and specialized microenvironment, called niche, that supports SC but varies in nature and location depending on the tissue type [5, 6]. Remarkable progress has been made in studies regarding the interaction between SC and their surrounding microenvironment in flies, *Caenorhabditis elegans*, and mammals. By comparing the SC niches in these systems, have emerged features and functions common to all [7]:

- The niche is composed of a group of cells in a special location that functions to maintain SC.

- The niche is a physical anchoring site for SC, and adhesion molecules are involved in the interaction between SC and the niche and between SC and the extracellular matrix.
- The niche generates extrinsic factors that control SC number, proliferation, and fate determination. Many developmental regulatory signal molecules, including Wnt, bone morphogenetic proteins (BMP), fibroblast growth factors (FGF), and Notch, have been shown to play roles in controlling SCl self-renewal and in regulating lineage fate in different systems.
- The niche controls normal asymmetrical division of SC.

Normally, at least in the hematopoietic, intestinal, and hair follicle systems, the niche maintains SC primarily in a quiescent state by providing signals that inhibit cell proliferation and growth [8]. Only upon receipt of a stimulating signal, SC become activated to divide and proliferate. Therefore, SC proliferation depends on dynamic niche signaling. Maintaining a balance between proliferation and anti-proliferation signals is the key to homeostatic regulation of SC, allowing them to undergo self-renewal while supporting ongoing tissue regeneration [9].

To identify the SC compartment was initially used Bromodeoxyuridine (BrdU) labeling, based on the assumption that SC divide infrequently and retain the DNA label for longer than the more rapidly cycling progenitor cells. This method was subsequently replaced by the identification of specific markers and the evaluation of the *in vitro* ability of SC to form rounded structures when cultivated in specific conditions. These structures have been named Sferoids; depending of the tissue of origin, it is possible to identify colonspheres (from colon), mammospheres (from mammary gland tissue), pneumospheres (lung tissue), neurospheres (from brain tissue) and so on. To date, many protocols have been described to produce in vitro spheroids from SC. The most common technique exploits SC embedding into a Matrigel compound that mimic the niche support. Otherwise it is possible to culture SC on non-adhesive surface such as coated plates that prevent adhesion, permitting SC to float in the medium (i.e. collagene or Poly 2-hydroxyethyl methacrylate-coated plates). Very recently, Sato *et al.* [10] and Jung *et al.* [11] first succeeded in isolating and expanding *in vitro* normal human colonic stem cells by an experimental protocol which entailed the use of a complex combination of several growth factors [10] and a

positive selection strategy based on the expression of the Ephrin type-B receptor 2 (EphB2) [11]. Thanks to this protocol, a single stem cell was able to form multicellular structures called organoids, since they presented crypt domains surrounding a central lumen lined by a villus-like epithelium ('villus domain').

1.2 Colon Stem Cells

The large intestine comprises the ascending colon, transverse colon, descending colon, sigmoid colon, rectum and anal canal. In general, the colon wall is composed of four histologically distinct layers; from inside to outside there are the mucosa, submucosa, muscolaris externa (muscle layer) and serosa. The innermost layer consists of a mucosa that includes the epithelium, lamina propria, and a thin layer of muscle (Figure 2). The simple columnar epithelium is folded to form a number of invaginations embedded in the connective tissue. These test-tube-shaped structures, called crypts of Lieberkühn, and containing approximately 2000–3000 cells/each [12], represent the functional unit of the colon involved in the absorption of water and vitamins.

The entire colon contains millions of self-renewing crypts, and it has been estimated that over $6x10^{14}$ epithelial cells are produced during the lifetime of an individual.

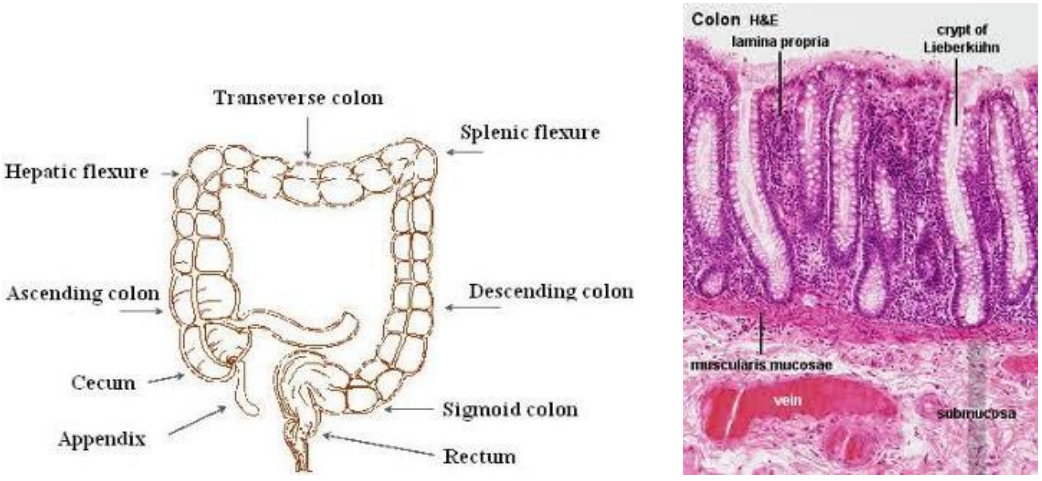

Figure 2: **Colon structure**. Anatomical components (left) and histology (right) of the colon [13].

The colon is organized in a hierarchical fashion and the epithelial layer is totally renewed every 5 days in humans [14]. The compartment of pluripotent stem cells is located at the crypt bases. The colon SC show unique properties as they remain in an undifferentiated state and produce epithelial cells that are committed to three different cell lineages within the colonic crypt compartment: **goblet** cells, **enteroendocrine** cells and **enterocytes**. The mucous-secreting goblet and the peptide hormone-secreting enteroendocrine cells belong to the secretory lineage whereas the enterocytes are members of the absorptive lineage.

SC usually give rise to two different daughter cells by asymmetric division to maintain normal crypt size and homeostasis [15]. After division, the daughter SC remains at the bottom of the crypt for guarantee self-renewal while the other is committed to TA status and start to migrate along the crypt wall to terminally differentiate at the crypt apex (Figure 3).

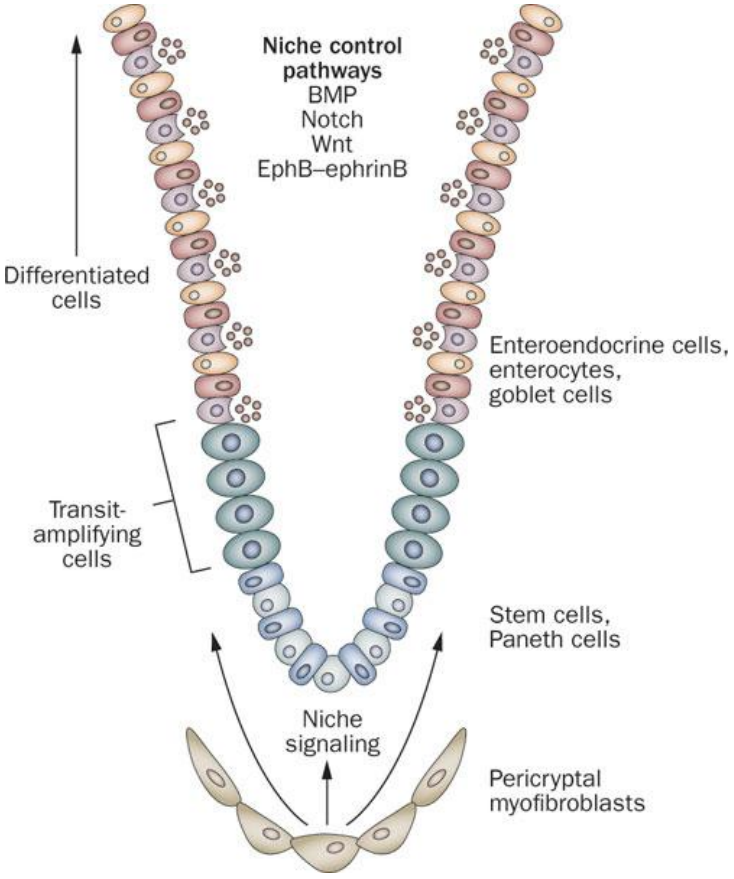

Figura 3. **Colon crypt organization**. Schematic representation of different cell population distribution along colon crypt. SC reside at the crypt bottom where they communicate with the niche cells - the pericryptal myofibroblasts. When in division, SC produce TA cells that start to migrate along the crypt wall to reach the apex once terminally differentiated [16].

1.3 Colon SC markers

In colon tissue, thanks to its architectural structure, the identification of putative SC markers has been favored by SC location at the bottom of the crypt.

Fujimoto and colleagues identified the integrin subunit β1 (**CD29**) as a candidate marker for the proliferative zone of the human colonic crypt, which includes SC and progenitor cells [17]. They demonstrated that the cells located in the lower third of the crypt expressed higher levels of CD29, compared to the cells in the remainder of the crypt.

A new marker for colon SC was identified in the Aldehyde Dehydrogenase 1 (**ALDH1**) enzyme. ALDH is a detoxifying enzyme that oxidizes intracellular aldehydes, thereby confering resistance to alkylating agents [18]. In fact, the detoxification capacity of ALDH, by protecting SC against oxidative insult, might underlie the well-recognized longevity of SC. ALDH also converts retinol to retinoic acid, a modulator of cell proliferation, which may also modulate SC proliferation. Immunostaining of human colon crypts showed that $ALDH1^+$ cells were confined to the crypt bottom, where SC are thought to reside [19].

The hyaluronic acid receptor **CD44** was also used in combination with the epithelial marker epidermal surface antigen (ESA) to identify and isolate colon SC. However, immunohistochemical analysis of normal colonic epithelium showed that CD44 expression occurred not only in cells at the crypt bottom, but also in cells within the proliferative compartment, where rapidly proliferating cells reside [20].

Another molecule identified as a putative human colon SC marker was Musashi-1 (**Msi-1**); Nishimura and his group demonstrated that only some cells at the crypt bottom expressed this marker [21]. Recently dublecortin CaM kinase-like-1 (**DCAMKL-1**), a microtubule-associated kinase expressed in postmitotic neurons, has been proposed as a putative colonic SC marker [22]. DCAMKL-1 was found expressed in the same cells as Msi-1, but likely represented a subset of Msi-1-expressing cells. In particular, $DCAMKL\text{-}1^+$ cells were found to be apoptosis-resistant following radiation injury.

B-lymphoma Mo-MLV insertion region 1 (**Bmi-1**) is a Polycomb Group (PcG) protein identified as an oncogene that regulates cell proliferation and transformation, and plays an important role in hematopoiesis and development of nervous systems.

Bmi-1 was first identified as small intestine SC marker and subsequently proposed as a colon SC marker [23].

In 2007 Barker and his colleagues [24] proposed Leucine-rich repeat-containing G protein-coupled receptor 5-positive (**Lgr5**) protein to define colon SC. This protein was first identified in mouse small intestine, where a single $Lgr5^+$ cell was demonstrated to be able to regenerate a complete crypt-like structure *in vitro* (in Matrigel support). Barker and his colleagues also demonstrated that each crypt contains approximately six long-lived stem cells intermingled with goblet cells in colon. Counter-intuitively, these cells were not quiescent, but divide every day. Their daughter cells constitute the TA crypt compartment that divides every 12–16 h, generating more or less 300 cells per crypt every 6 day. They reside within crypts for approximately 48 h, undergoing up to five rounds of cell division while migrating upwards. During the differentiation process, the committed TA cells reach the crypt apex, where they rapidly die as totally differentiated cells [25].

Thus, despite that several colon SC markers have been recognized, it is as yet impossible to define a specific phenotype for colon SC: depending on the techniques used for SC isolation, culture and analysis, and depending on the surface marker used, the percentage of SC in human colon samples ranges from 0.1 to 10%. Furthermore, according to the different marker expression it seems that two different populations of SC could be recognized: a SC compartment in a quiescent state (i.e. $DCAMKL\text{-}1^+$ cells) and an actively cycling population (i.e. $Lgr5^+$ cells also called Crypt Basal Columnar (CBC) cells.

Marker	Other name	Function	References
CD29	Integrin b1	Cell adhesion molecule	17
ALDH1	ALDC	Enzyme	18, 19
CD44	CDW44	Cell adhesion molecule, Hyaluronic acid receptor	20
Lgr5	GPR49	Unknown, Wnt target gene	24, 25
Msi-1		RNA binding protein	21
DCAMKL-1		Kinase	22
Bmi-1		Transcript repressor	23

Table1. **Normal colon SC markers.** List of SC markers identified in human normal colon tissue.

1.4 Musashi-1

Among the different colon SC markers, Musashi-1 (Msi-1) looks as the most interesting and promising marker. Msi-1 is a RNA-binding protein initially recognized as a protein required for asymmetric divisions of sensory organ precursor cells in *Drosophila* [26]. The name Musashi is a tribute to the famous 17^{th} century Samurai, Miyamoto Musashi, who developed the two swords technique that recalls Msi-1 three-dimensional structure.

Through immunohistochemical analysis Msi-1 expression has been observed in neural precursor cells of the developing central nervous system (CNS). In 1998 it was recognized as a marker for stem cells of the CNS, while only in the 2003 Nishimura and colleagues [21] demonstrated that the expression of Msi-1 in normal colon mucosa was restricted to the lower part of the crypt, where *bona fide* stem cells reside. In the next years Msi-1 has been described as a marker of adult stem cells and progenitors in other tissues such as hair follicles [27], intestine [28] and mammary gland [29].

Msi-1 acts by binding the sequences present in the 3'-untranslated region (3'-UTR) of target mRNA thereby, repressing their function at the translational level [30]. Msi-1 represses the translation of mNumb [31], a negative regulator of Notch pathway, $p21^{Cip1}$, an inhibitor of cycling-dependent kinase [32], and doublecortin (Dcx) a microtubule-binding protein involved in neural stem cell migration [33]. These latter mRNA targets are both implicated in cell proliferation and protein modification. It has been demonstrated that $p21^{Cip1}$ is absent in Msi-1-expressing cells, which is in agreement with the ability of Msi-1 to block its translation. $p21^{Cip1}$ is believed to function as a rheostat to maintain a balance between stem cell quiescence and stem cell exhaustion resulting from increased cell cycle entry.

2. CANCER STEM CELLS

2.1 Identification and origin

Within tumor masses it has been recently identified a small cell population called "tumor initiating cells". These cells present the ability to re-grow the tumor from which they were isolated. Several studies have revealed that these cells have the capacity of self-renewal, the potential to develop into any cell in the overall tumor population and the proliferative ability to drive continued expansion of the population of malignant cells. Since the properties of such tumor initiating cells mirror those of normal stem cells, in the 1990 was introduce the term Cancer Stem Cells (CSC) to better identified such malignant cell population.

The origin of CSC is still a matter of debate. It is possible that CSC arise from mutations that occur in a normal stem cell. However, several lines of evidence indicate that CSC could also originate from mutated TA cells. These cells posses substantial replicative ability, but they do not usually have the self-renewal capacity of stem cells (Figure 4). To become CSC, a TA progenitor cell must acquire mutations that confer the property of self-renewal [34]. In any case, a general consensus exists that CSC are essential for tumor initiation, progression and maintenance.

Different approaches have led to the identification of CSC: (I) examination of the expression of tissue-specific surface markers such as CD44, CD133, CD24 which are selectively expressed on CSC but not on the bulk of tumor cells; (II) examination of specific functional features of CSC and (III) evaluation of their tumorigenic potential when injected into immunocompromised mice at low number. In reference to this point, the most common approach to isolate CSC from total tumor population is FACS sorting, based on the expression of specific surface antigens recognized as stemness markers. Once isolated, CSC are injected in scalar number into immunodeficient mice and their tumorigenic potential is compared with the ability to form tumors by the same number of non SC.

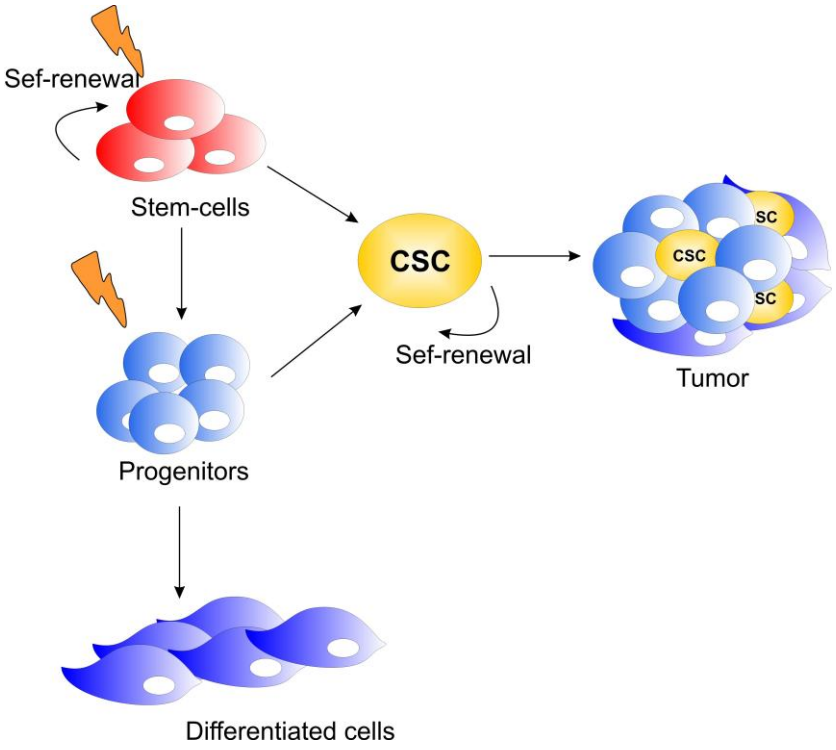

Figure 4. **Cancer Stem Cells origin**. Mutations can occur in normal SC inducing a neoplastic transformation, but can also occur in progenitor cells that acquire stemness properties such as indefinite proliferative potential and self-renewal.

2.2 Characterization

In some studies CSC have been recognized by dual-wavelength flow cytometry as the so-called Side Population (SP) on the basis of their ability to extrude the fluorescent DNA-binding dye Hoechst 33342 [35]. A SP has been identified in both several tumors and established cancer cell lines. In breast cancer cell lines, the SP population is characterized by a number of features, including an $ALDH^+/CD44^+/CD24^-$ phenotype, spheroid formation ability, clonogenicity, multilineage differentiation potential and tumor initiating capacity upon injection into NOD/SCID mice [36]. Similar properties were attributed to SP cells isolated from DAOY and PFSK medulloblastoma cell lines that contained a small population (1.9%) of $CD133^+/Nestin^+$ cells able to form spheroids in vitro and to generate xenograft tumors [37].

A further approach to identify CSC is based on their replicative potential: under standard culture conditions CSC are poorly or non-proliferating cells compared to the bulk of tumor cells. By measuring fluorescence intensity following labeling with membrane-binding dyes such as PKH26, it is possible to identify cells that proliferate

and eventually loose the dye from cells that remain in quiescent state hence maintain high intensity of the dye. This technique was recently utilized by the Pelicci's group [38] to identify breast cancer stem cells, recognized as $PKH26^{high}$ cells.

A large fraction of CSC is likely in a quiescent state and do not respond to conventional chemotherapeutics that kill proliferating cells (Figure 5); CSC could thus represent the reservoir of drug-resistant cells responsible for relapse after a chemotherapy-induced remission. It has been shown that the $CD133^{-}$ fraction of human colorectal cancer cells showed a dose-dependent sensitivity to oxaliplatin and/or 5-Fluorouracil (5-FU), whereas the $CD133^{+}$ fraction, sorted from the same samples, did not undergo drug-induced apoptosis, even by increasing drug concentrations [39]. These behavior could be attributed to the fact that CSC exhibit a high expression of ATP-binding cassette (ABC) transporters, especially BCRP (breast cancer resistance protein or ABCG-2) and MDR1 (multi-drug resistance-1, ABCB1 or P-glycoprotein) as part of their self-protection capabilities [40]. ABC transporters can power the translocation of substrates across biological membranes against a concentration gradient through hydrolysis of ATP and are currently be associated with drug resistance. However, ABC transporters are not the sole cause of drug resistance in CSC; several other factors, such as the CSC capacity of DNA repair and their quiescent state, may also have a key impact on drug resistance [41].

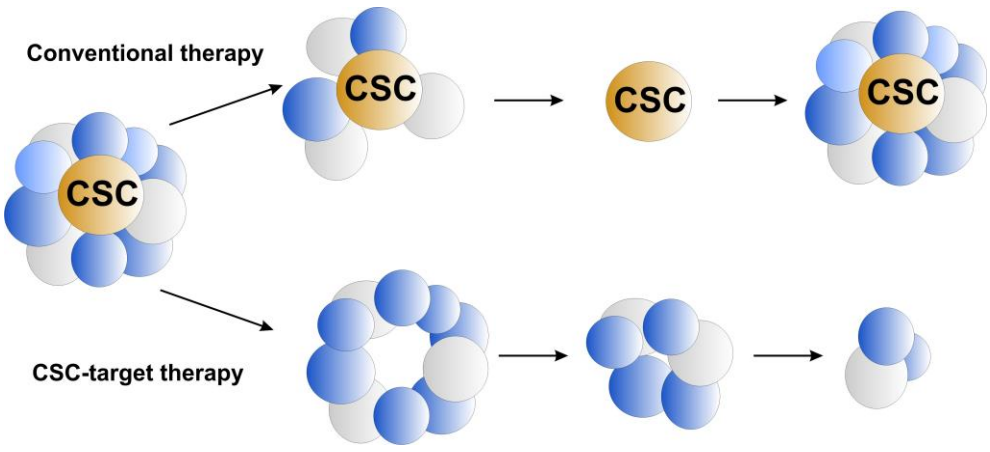

Figure 5. **Traditional *versus* new cancer therapies**. Conventional therapy such as chemotherapy kills tumor cells but not CSC that can drive tumor relapse. An hypothetical CSC therapy should address to specific features of CSC, thus once eliminate the stem counterpart, tumor loses ability to generate new cells and degenerate.

2.3 Colon CSC markers

As for normal SC, CSC are fundamentally isolated thanks to the expression of specific markers. The first marker identified for colon CSC was **CD133,** a pentaspan transmembrane glycoprotein also known in humans as Promin-1. Ricci-Vitiani and colleagues [42] and O'Brien and colleagues [43] reported that the $CD133^+$ cell subset in colorectal carcinoma (CRC) could induce xenograft tumors when injected into NOD/SCID mice, a property strictly related to stemness. However, it was subsequently reported that CD133 expression is not specific to colon CSC: both CSC and progenitors expressed this marker, and both $CD133^+$ and $CD133^-$ metastatic colon cancer cells were able to initiate tumors [44]. Some years later, Dalerba *et al.* suggested that **CD44** and **EpCAM** could represent more robust markers than CD133, as CD44 expression could also be detected in tumor cell populations that score negative for CD133 expression [45]. Analysis of the surface molecule repertoire of $EpCAM^{high}/CD44^+$ cells led to the identification of CD166 as an additional differentially expressed marker, useful for CSC isolation in three of three CRC tested [45]. It has also been demonstrated that some markers identified in normal colon SC are highly expressed in neoplastic tissues and could be considered as possible CSC markers (i.e. **Msi-1** [46], **Lgr5** [47] and **ALDH1** [48]).

It has been recently demonstrated that none of the putative markers (CD44, CD133, CD166 and EpCAM) could define CSC, since CSC isolated according to their expression did not exhibit increased survival when treated *in vitro* with chemotherapeutic drugs, nor did they display higher tumorigenicity in vivo [49].

Marker	Other name	Function	References
CD133	Prominin 1	Tumor angiogenesis	42, 43
CD44	CDW44	Cell adhesion molecule, Hyaluronic acid receptor	45
EpCAM	ESA	Cell Adhesion molecule	45
Msi-1		RNA binding protein	46
Lgr5	GPR49	Unknown, Wnt target gene	47
ALDH1	ALDC	Enzyme	48
CD166	ALCAM	Cell Adhesion molecule	45

Table 2. **Colon CSC markers.** List of CSC markers identified in human tumoral colon tissue.

3. COLORECTAL CANCER

3.1 Neoplastic Progression

CRC accounts for approximately 150.000 new cases and 56.000 deaths per year in the United States, making it the third most common cause of death among men and woman [50].

It has been suggested that CRC could follow multistep model of neoplastic transformation since the transformation of normal mucosal epithelia to invasive colorectal carcinoma occurs via a well-coordinated accumulation of mutations in a series of critical genes [51]. The first event that occurs during the neoplastic progression is the acquisition of a mutation in the *adenomatous polyposis coli* (APC) gene. APC is a tumor suppressor gene that controls the Wnt/β-catenin signaling pathway, and its loss translates into accumulation of nuclear β-catenin, leading to the constitutive activation of Wnt cascade. Wnt activation is associated with aberrant crypt cell proliferation; these cells are unable to exit the crypt and start to expand sideways forming hyperplastic or dysplastic tissue. The transition from a dysplastic crypt to the so called "intermediate adenoma" necessitates an additional mutation that in 50% of the cases involves the Kras gene. KRAS is a small GTP-binding protein that transduces signals from surface receptors to the nucleus (Fig 6). As adenomas continue to grow and begin to show great histological disorder, there is the gradual accumulation of additional mutations in oncogenic genes such as Smad4, Smad 2 and DCC. By the end, loss of functional P53 by damage to both alleles drives progression to carcinomas. P53 is a fundamental oncosuppressor gene, able to suppress cell division and to induce apoptosis in response to stress or damage; its malfunction seems to be related to tumor invasiveness and metastatic ability [52].

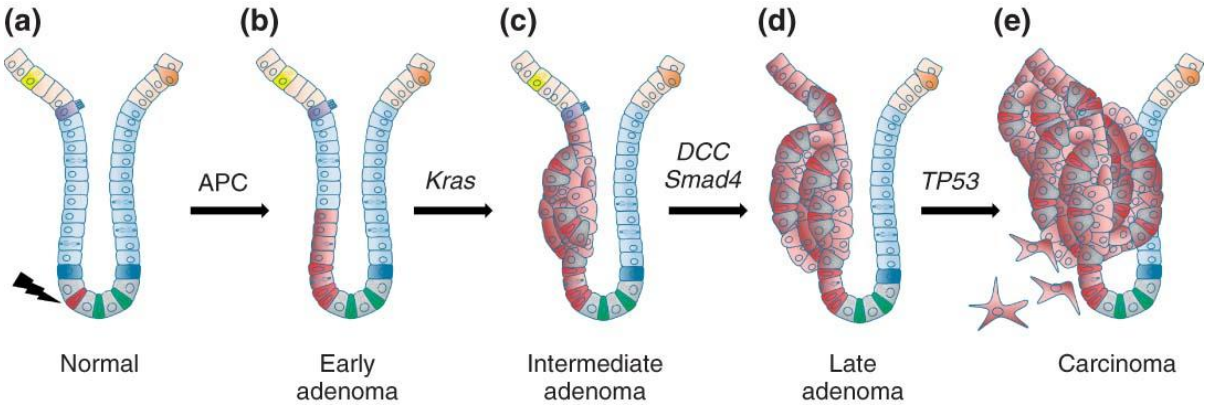

Figure 6. **Model of intestinal cancer initiation and progression.**
Progression from normal epithelium to colorectal carcinoma occurs through adenoma formation. Mutations in *APC* are the first event that mediates the transition of single pre-neoplastic cells to aberrant crypt foci that develop into adenoma and colorectal carcinoma due to mutations in other oncogenes and tumor suppressor genes such as *Smad, p53, K-ras* [53].

2.2 CSC model for neoplastic origin

According to the literature there are currently two models that explain the cellular origin of cancer:

1) The hierarchical model (o CSC model)

2) The stochastic model.

The CSC model suggests that tumors grow like normal tissues of the body, with SC at the starting point of a hierarchical system that produces new cells to make tissue grow. According to this idea, tumors contain CSC that divide and feed tumor growth. These cells can self-renew extensively and produce mature TA cells which divide and differentiate into specialized tumor cells. These specialized tumor cells are no longer able to divide, and so they do not contribute to tumor growth. According to this idea, the cells in a tumor are organized in a strictly hierarchical fashion, with CSC at the top of the tree, giving rise to all other cancer cells.

In the stochastic model, instead, all cancer cells have the same potential to grow and divide, but each cell chooses at random between self-renewal and differentiation. The cells in tumor are not arranged in an organized system, and any cell could have the same intrinsic potential to contribute to tumor growth. Different types of cancer may work in different ways, so it is possible that both of these theories are right.

The CSC model could be more relevant in the explanation of colon cancer origin. In fact, CSC are long-lived cells in the colonic crypt, and thus could accumulate

cancer-causing mutations over years or decades. Histological evidence from colon tumors indicates that they have multiple differentiated cell types, suggesting a SC origin for colon tumors, because only multipotent SC could give rise to so many different types of cells within the tumor.

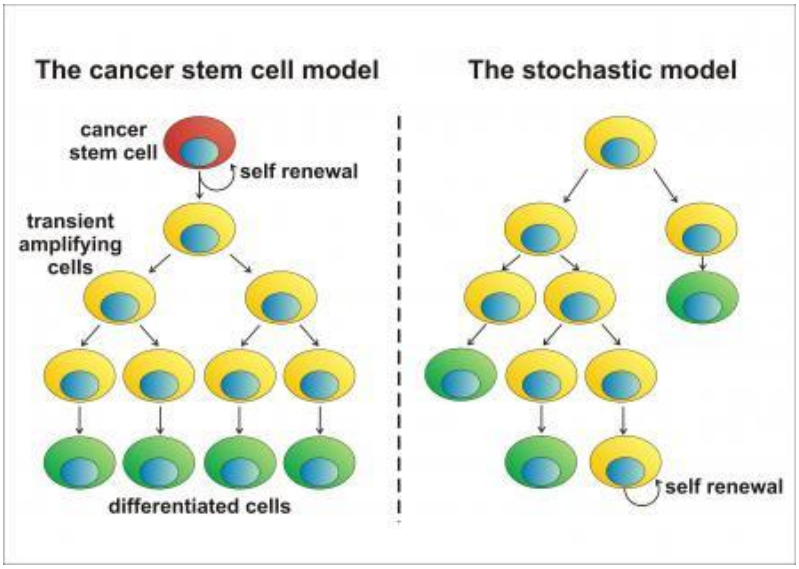

Figure 7. **Models for cellular origin of Cancer**. The cancer stem cell theory suggests a clear hierarchical cell organization within a tumor, with SC at the top. The stochastic model, instead, describes tumor growth as a random process due to contribute of all different cell types.

3.3 Metastatic process

The metastatic process is due to some cancer cells that, according to a complex sequence of biological events leave the primary tumor site, enter the lymphatic or circulatory system, survive within the circulation flow, overcome host defenses, extravasate and then grow as a metastatic tumor [54].

Cancer cells, probably CSC, undergo a process named EMT (Epithelial to Mesenchymal Transition) through which they acquire migration ability, invasiveness and mesenchymal morphology. These features permit EMT cells to dissolve adherent and tight junctions, loose cell polarity and invade stromal compartment thanks to the action of matrix metallopreoteinase (MMP) that drive the degradation of ECM releasing growth factors that stimulate cell proliferation [55].

Once in the stroma, cancer cell aggressive behavior is enhanced by various types of signals such as secretion of cytokines or stimuli from tumor-associated macrophages (TAM) that drive cell entry into the lumina of lymphatic or blood vessels. Intravasation can be facilitated by molecular changes that promote the ability of cancer cells to cross the pericyte and endothelial cell barriers that form the walls of microvessels. Within the lumina, cancer cells disseminate through the venous and arterial circulation as Circulating tumor cells (CTC), surviving to a variety of stresses to reach distant organ sites; CTC interact with leukocytes and aggregate with platelets, which protect cancer cells against mechanical stress and leukocytes. At this point CTC extravasate in specific tissues where microvessel permeability is low due to factors released from primary tumor that induce vascular hyperpermeability, thus creating a "premetastatic niche" (Figure 8).

Depending on the site of primary tumor, CTC form metastases in specific organs; to date this is a major unresolved issue. It has not known as yet whether CTC tropism is due to specific ligand-receptor interactions, between CTC and luminal walls of the microvasculature, or to cytokines released from specific organs where CTC metastasize. It is also possible that their localization is simply due to CTC arrest in the circulatory flow imposed by blood vessels diameter or capillary size and restrictions.

When arrived in anew location, CTC cells switch from mesenchymal to epithelial morphology (from EMT to MET [56]). Here metastatic cancer cells can remain in an apparent long-term dormancy (defined as "tumor dormancy") until they start to proliferate again, eventually inducing new vessel formation for metastatic mass feeding.

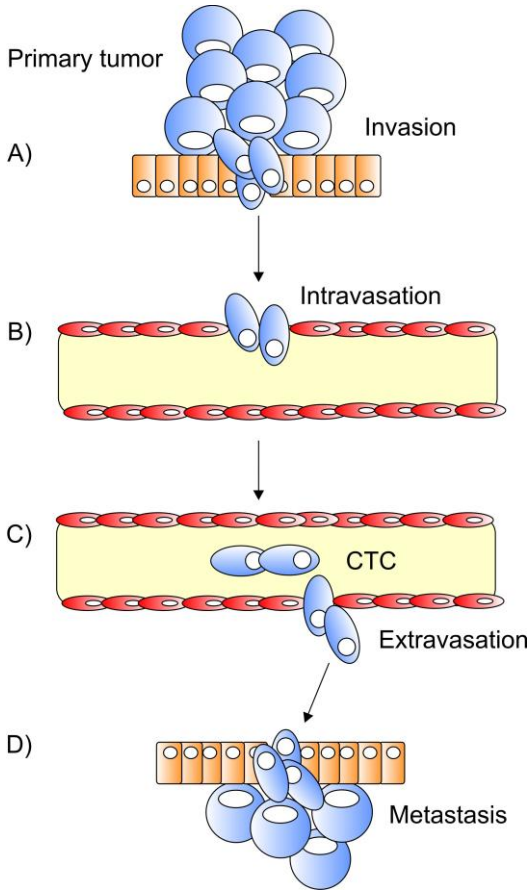

Figure 8. **Metastatic process**. (A) From primary tumor mass, few cells detach, invade stroma and (B) intravasate into the lumina of blood or lymphatic vessels. (C) Once in the venous and arterial circulation these cancer cells are called CTC; when arrived in target organs CTC arrest and extravasate inducing (D) metastatic growth and formation of a secondary tumor in the new appropriate environment.

4. THE NOTCH PATHWAY

4.1 Pathway description

The *Notch* gene was first recognized in a mutant *Drosophila* with an indentation in the wings. In the 1930s, it was suggested that the genetic locus responsible for this phenotype played an important role in the cell fate decision during *Drosophila* embryogenesis and that the homozygous mutation of this locus resulted in excessive differentiation to neuronal tissue.

Only in the 1980s molecular cloning studies revealed that the *Notch* gene encodes a transmembrane protein that functions as a receptor for the ligand present on the cell surfaces of neighboring cells [57]. In mammals, Notch signals through four different receptors (Notch1-4) and 5 different ligands. A prototypical Notch

gene encodes a single transmembrane receptor composed by an extracellular, a juxtamembrane, a transmembrane and a cytoplasmic region. The extracellular region presents a conserved array of up to 36 epidermal growth factor (EGF)-like repeats, involved in ligand interaction, followed by a cysteine-rich Notch or LIN12 (LN) domain. The juxtamembrane region is characterized by specific proteinase cleavage sites; the transmembrane region includes a cleavage site while the cytoplasmic region contains several functional domains. Furthermore, the cytoplasmic region is composed by a RAM (RBP-Jκ- associated molecule) domain, a set of six ankyrin (ANK) repeats flanked by two nuclear localization sequences (NLSs), and by a transactivation (TAD) domain, which is present only in Notch1 and Notch2 but not in Notch3 or Notch4 receptor. Finally, the last domain (PEST) is composed by a tail rich in proline, glutamate, serine and threonine [58].

The five transmembrane ligands that interact with Notch receptors, Delta-like ligand 1 (DLL1), DLL3, DLL4, Jagged 1 (JAG1) and Jagged 2 (JAG2), share structural homology, including a DSL domain (Delta, Serrate and LAG2), followed by a number of EGF-like repeats (six in the case of DLL3, eight in the case of DLL1 and DLL4, and 18 in the case of JAG1 and JAG2) [59], with a cysteine-rich (CR) domain found only in JAG1 and JAG2, followed by a transmembrane domain and a short cytoplasmic tail [60].

As shown in Figure 9, the Delta/Jagged–Notch pathway uses a distinct molecular mechanism to transduce a signal from the cell surface to the nucleus, and thus to regulate expression of target genes. After binding to a Delta ligand, the Notch receptor undergoes a series of proteolytic events near the cell surface, including the S2 cleavage mediated by A-Disintegrin And Metalloproteinase 10 (ADAM10) or TNF-α-converting-enzyme (TACE; also known as ADAM17), followed by the S3 cleavage mediated by the γ-secretase enzyme complex, resulting in the release of the Notch intracellular domain (NICD) which then translocates to the cell nucleus [61]. Once in the nucleus, NICD binds to CSL1 and converts it from a transcriptional repressor to an activator. Active CSL1 interacts with one of three transcriptional regulators MAML-1, and p300⁄CBP, helping to convert the transcriptional co-repressor (Co-R) complex into an activator complex, and thus induces the expression of a panel of target genes [62].

The NICD–RBP-Jk complex up-regulates expression of primary target genes of Notch signaling that belong to the bHLH family. These proteins are characterized by the presence of an Helix-Loop-Helix motif (HLH) and by a DNA-binding basic domain. In mammals there are two distinct Notch target families:

1) Hes (*Hairy/Enhancer of Split*)

2) HRT (*Hairy-Related Transcription factor*), also known as Hey.

Both Hes and Hey are transcriptional repressors and appear to act as Notch effectors by negatively regulating expression of downstream target genes [63].

In addition, Notch signaling is positively regulated by Musashi-1 that acts binding Numb, an inhibitor of NICD nuclear translocation, eventually causing its deregulation [64].

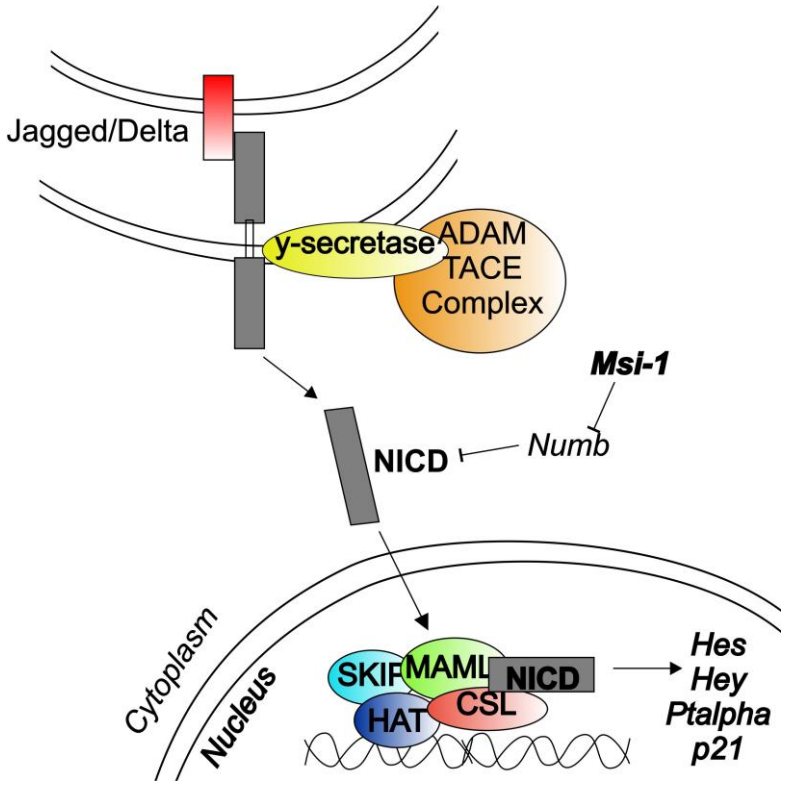

Figure 9. **The Notch Pathway.** Following cell-to-cell contact, Delta or Jagged ligands bind Notch receptor thus inducing its proteolytic cleavage. NICD is released into the cytoplasm and translocates to the nucleus where it acts as a transcriptional activator of Notch-associated target genes, including members of HES and HEY family, Ptα and p21. NICD nuclear translocation is allowed by Msi-1 binding of Numb mRNA and the consequent inhibition of Numb function.

4.2 Notch Pathway in normal colon mucosa and SC

In colonic tissue, the Notch pathway plays a central function in the intestinal cell fate decisions (Figure 10), in fact it is essential to maintain the crypt compartment in its undifferentiated and proliferative state. In the colon, abundant expression of Notch1, Jagged1 and Hes1 was observed in the proliferative zone located within the middle-third of the crypt. On the contrary, low levels of Notch1 and Hes1 were detected at crypt apex, where differentiated epithelial populations are present [65].

Notch involvement in the intestinal epithelial differentiation was investigated by inhibition of the pathway. Conditional deletion of the CSL gene or pharmacological inhibition of γ-secretase resulted in the rapid and complete conversion of all epithelial cells into goblet cells [66]. On the contrary, gain of function through specific over-expression of a constitutively active Notch1 receptor resulted in depletion of goblet cells and reduction in enteroendocrine cell differentiation [67].

Furthermore Riccio *et al*. showed that conditional inactivation of both Notch1 and Notch2 receptors in the gut resulted in the complete conversion of the proliferative crypt cells into post-mitotic goblet cells [68]. The same effect could be observed in intestinal tumors arising in Apc^{min} mice following inhibition of the Notch pathway [66].

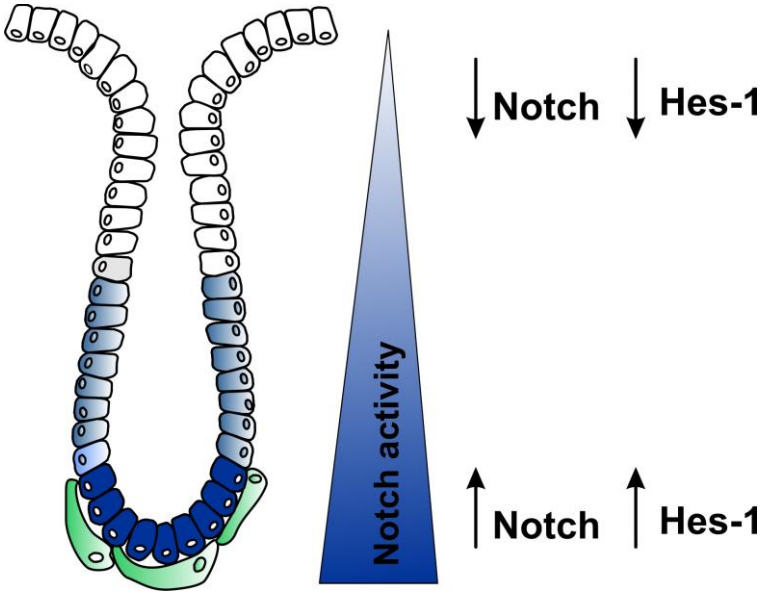

Figure 10. **The Notch signaling pathway in colonic crypt**. Notch activation is mainly restricted in the proliferative zone located in the lower region of the crypt. Moving along the crypt wall toward the apex, the levels of Notch and his target gene Hes-1 reduce.

As far as the genes controlled by Notch during colon differentiation are concerned, it has been demonstrated that differentiation into **goblet** cells is regulated by Atoh1- kruppel-like factor 4 (Klf4) pathway, which translates into activation of expression of the gastrointestinal mucin (*Muc2*). Indeed, Notch target gene Hes1 represses transcription of the bHLH transcription factor Atoh1, which is directly regulated by the Wnt pathway. $Hes1^{-/-}$ animals are embryonic lethal, but the intestines from these animals show an increase in goblet, and enteroendocrine cells, as well as a decrease in absorptive enterocytes [69, 70]. Likewise, differentiation into **enteroendocrine** cells is guided by Neurogenin3 (Ngn3) that is located downstream of the Notch-Hes1-Atoh1 cascade; mice homozygous for a null mutation in Ngn3 transcription factor do not develop any intestinal endocrine cells [71].

Finally, **enterocyte** differentiation is driven by E47-like factor 3 (Elf3), which is a target of Hes1 and a member of the Ets transcription family. Indeed, mice homozygous for an Elf3 null mutation die shortly after birth and display poorly polarized enterocytes that have not reached maturity [72].

Thus, all these evidences show that the Notch pathway controls absorptive *versus* secretory fate decisions in the intestinal epithelium [73] as well as proliferation of undifferentiated compartment *versus* cells differentiation.

4.3 Notch in CSC: Therapeutic Implication

Aberrant Notch activation has been demonstrated in CSC from several tumors, including glioma [74] , breast [75], colon [76] and pancreatic cancer [77]. Pancreatic CSC, identified by the expression of CD44, CD133, CD24, CD34 and ALDH, showed higher levels of Notch-1 and Notch-2 mRNA associated to the loss of microRNA-34 (miR-34), compared to pancreatic non-CSC [77]. Since Notch-1 and 2 are downstream targets of miR-34, these results suggest that miR-34 could be involved in pancreatic CSC self-renewal via modulation of Notch activity. Further data support a role of other miRs in the regulation of Notch levels in pancreatic CSC. Li *et al.* observed low miR-200 levels in gemcitabine-resistant pancreatic cancer cells showing canonical features of CSC; moreover, its forced expression significantly inhibited Notch signals [77]. Thus, modulation of specific miRs could be a successful strategy to target certain CSC features, such as drug resistance.

In colon cancer cells with CSC properties, inhibition of Notch-1 induced a reduction in cell proliferation, a cell cycle arrest in G_0-G_1, and it increased the number of apoptotic cells. Moreover, Notch inhibition reduced both spheroid formation in vitro and tumorigenic capacity in mice, two established CSC features. In contrast, Notch-1 overexpression increased cell proliferation, cell cycle progression and it reduced apoptotic cells [78].

Another approach to inhibit Notch signalling is to use a γ-secretase inhibitor (GSI), such as GSI-18, to enhance the efficacy of temozolomide monotherapy as demonstrated in $CD133^+$ glioma CSC [79]. In culture GSI reduced the CSC population also in some medulloblastoma cell lines [80] : in fact a 3-fold reduction of the $CD133^+$ stem-like fraction was cobserved in DAOY cells treated with GSI as well as in other medulloblastoma cell lines (D283Med, D425Med and PSFK). On the contrary, forced expression of Notch2 intracellular domain (NICD2) in DAOY cells increased the $CD133^+$ fraction to > 17%. Similar results were obtained by analyzing the SP in these cell lines: constitutive activation of Notch2 led to a 4-fold increase of SP cells, whereas Notch inhibition almost completely ablated SP. In the same study, the CSC fraction expressing the neural stem cells marker Nestin was also analyzed; NICD2 activation increased the $Nestin^+$ cell fraction from 10% to 47%, whereas Notch blockade by GSI reduced this population to about 2.4%. These findings buttress the plasticity of the CSC phenotype, a concept which has found experimental support in the last two years.

The main problems associated with GSI is gastrointestinal cytotoxicity; for this reason, several “non-toxic natural agents” able to modulate Notch signalling, such as curcumin, quercentin, isoflavone, and sulforaphane are being tested.

More promising approaches are offered by antibodies targeting either Notch receptors or Notch ligands. Hoey *et al.* showed that a neutralizing antibody against DLL4 decreased by 50% colon CSC population, defined as $ESA^+/CD44^+/CD166^+$ cells. Notably, the combination of anti-DLL4 and Irinotecan further decreased the percentage of CSC in treated tumors, whereas Irinotecan monotherapy induced an increase from 28% to 43% of the $ESA^+/CD44^+/CD166^+$ population [81]. Dontu and colleagues [82] evaluated the effect of Notch signaling agonists and antagonists on breast CSC, cultured either as floating mammospheres or on a collagen matrix, under conditions that promote differentiation. A synthetic peptide derived from the Delta-

Serrate-LAG 2 (DSL) domain conserved in all Notch ligands and a recombinant Delta 1 ligand fused to the immunoglobulin Fc fragment were utilized as agonists of Notch signaling, whereas a Notch4-specific antibody or a GSI were used as antagonists. After treatment with agonists a 10-fold increase in mammosphere formation was observed, compared to control cultures; this effect was abrogated by anti-Notch 4 antibody or GSI, while these treatments had no effects on differentiated mammary epithelial cells.

AIM

Aim of this paper is to address the *in vitro* culture and characterization of distinct epithelial cell subsets from normal human colon mucosa. In general, previous attempts to grow in long-term culture cells with stem-like properties from normal human colon mucosa had been unsuccessful. Very recently, however, Sato *et al.* [10] and Jung *et al.* [11] succeeded in isolating and expanding *in vitro* normal human colonic stem cells by a positive selection strategy targeting the expression of EphB2. In this work, we instead adopted a totally different strategy, and chose to derive cells endowed with stem-like properties by simply exploiting their proliferation rate.

Once described a stem-like cell population in normal colon tissue, we turned to tumoral and metastatic colon samples, to identify possible features in such population that could be helpful in understanding neoplastic progression and stem cell involvement.

The involvement of the Notch pathway in stem cells maintenance and the overexpression of one of its receptor, Notch3, in tumoral and metastatic colon tissue has been reported [83]. On the other hand, the activation of Notch intracellular domain is due to the action of Msi-1, a colon stemness marker, and to date nothing is known about its regulation. Based on these considerations, we tried to describe a possible modulation of Msi-1 by Notch3 receptor using a specific metastatic cell line, MICOL-14^{tum} cells, and primary human metastatic samples.

MATERIAL AND METHODS

1.Primary samples and cell lines

Following informed consent, 80 histologically normal samples, 5 tumoral colonic mucosa samples and 20 liver CRC metastatic samples were obtained from colon cancer-bearing patients undergoing colectomy. Immediately after resection, the tissues were washed in cold phosphate-buffered saline (PBS) containing Penicillin/Streptomycin, gentamicin (1 µl/ml) and amphotericin (1.25 µg/ml). Each samples was divided in two parts: one fragment was snap-frozen in liquid nitrogen, and stored at -80°C until use, while the other was processed as described elsewhere [84]. Briefly, the tissue was minced and incubated for 3 h at 37°C with collagenase (1.5 mg/ml) and hyaluronidase (20 µg/ml) in DMEM/F12 medium (Gibco, Invitrogen, Carlsbad, CA). The digested material was centrifuged and sequentially filtered through 70 and 40 µm filters; red blood cell lysis was performed at 37°C for 7 min in NH_4Cl/ $KHCO_3$/EDTA buffer, and cell viability was assessed by Trypan Blue dye exclusion. The cell suspension was then plated in serum-free DMEM/F12 medium and maintained at 37°C in a 5% CO_2 humidified atmosphere in low adhesion plate for 1 week. All experiments were performed after a week of reduced adhesion condition.

The MICOL-14^{tum} is a tumorigenic variant of MICOL-14 cells, a cell line derived from a lymph node metastasis of rectal cancer [85]. MICOL-14^{tum} has been obtained from a tumor developed in NOD/SCID mice after subcutaneus (s.c.) injection of parental MICOL-14 cells in Matrigel plus bFGF (100 ng/ml; PeproTech, London) and interleukin-8 (100 ng/mL) [86]. Cells were grown in RPMI 1640 medium supplemented with 10% FCS and 1% L-glutamine (Invitrogen, Milan, Italy) and used within 6 months from thawing and resuscitation.

2. *In vitro* cell culture and PKH26 staining

Isolated cells from human colon mucosa specimens were plated at the concentration of $2x10^5$ cells/ml in untreated ultra-low adhesion 6-well plates (BD Falcon, Franklin Lakes, NJ) and cultured in serum-free DMEM/F12 medium

supplemented with Pen/Strep, glucose (6 mg/ml), $NaHCO_3$ (1 mg/ml), HEPES (5 mM), L-Glutamine (2mM), heparin (4 µg/ml), bovine serum albumin (BSA; 4 mg/ml), insulin (25 µg/ml), anhydrous sodium selenite (30 nM), progesteron (20 nM), apo-transferrin (100 µg/ml), epidermal growth factor (EGF; 20 ng/ml, PeproTech), basic fibroblast growth factor (bFGF; 10 ng/ml, PeproTech), and putrescin (9.6 µg/ml, SigmaAldrich, St. Louis, MO).

After one week the cells were collected, washed with DMEM/F12 medium and incubated for 3 min with a 1:250 (v/v) PKH26 solution (Sigma-Aldrich,) [87]. The staining was blocked with 1% BSA and DMEM/F12, and the cells were seeded in poly-2-hydroxyethyl methacrylate (PhEMA)-coated plates in the absence of serum at $2x10^4$ cells/well. According to the proliferation curve, the medium was replaced every 7 days. The plates were examined daily by phase-contrast microscopy to evaluate the formation of spheroid-like structures, and pictures were acquired with a Nikon camera. PKH26-stained cells were also observed with fluorescence microscope and pictures acquired with an Olympus camera or confocal microscope (Axiovert 1000M, Zeiss, Schwabhausen, Germany).

3. Colony formation assay

To address the frequency of spheroids-forming cells we performed an extreme limiting dilution assay (ELDA) in the presence or absence of α-Notch2/3 mAb (1µl/ml). Briefly, primary colon samples and MICOL-14^{tum} cells were plated at different concentrations in 96-well flat-bottom ultra-low attachment PhEMA-coated plates (BD Falcon) in a total volume of 0.2 ml of medium described above for primary cells and RPMI 1640 serum-free supplemented with EGF and bFGF for MICOL-14^{tum}cells. At least 30 replicates were set up for each cell concentration. According to experimental design, after 4 or 10 days of incubation at 37°C, 5% CO_2 wells were scored for outgrowth of spheroids; the frequency of spheroids-forming precursors in each population was calculated using ELDA web tool at http://bioinf.wehi.edu.au/software/elda. For normal samples cells were collected at the 2^{nd} week of culture and ELDA was performed in both unfractionated and FACS-sorted PKH^{pos} cells.

4. *In vitro* cell differentiation

To promote *in vitro* cell differentiation, cells maintained in serum free conditions were FACS-sorted at the 3rd week of culture into PKH^{pos} and PKH^{neg} subsets, and included into Matrigel (BD Biosciences) or transferred to untreated 24-well plates, in the presence of 10% fetal calf serum (FCS, Invitrogen) and in the absence of bFGF and EGF. In both cases, the cells were plated at a density of $5x10^4$ cells/ml. For Matrigel cultures, 24-well plates were dispensed with Matrigel-included cells and layered with DMEM supplemented with 10% FCS. The cells were maintained at 37°C in a 5% CO_2 humidified atmosphere, and the medium replaced every 2 days.

5. Flow cytometry (FACS) analysis

According to the experimental design cells were collected weekly or after 72h of treatment with α-Notch antibodies. Cells were washed in PBS and PKH26 intensity (were present) measured by FACS (LSR II, BD Biosciences). The expression of CK18 (1:200; Abcam, London UK), CK20 (1:10; Dako, Milan, Italy), Lgr5 (1:400; Origene, Rockville, MD), and Msi-1 (1:200; Abcam) was measured by single staining or with the appropriate antibody combinations in fixed cells. Cells were fixed in 4% Paraformaldehyde and permeabilized with 0.1% Triton X-100. Unspecific binding was prevent by saturation with PBS/5% BSA followed by incubation with the primary antibody and then with the appropriate secondary antibodies (Alexa 1:500, Invitrogen) [88]. Data were collected from at least $5x10^4$ cells/sample and analyses were performed with Flow Jo (TreeStar, Ashland, OR). Cell viability was evaluated by Live/Dead (Invitrogen) staining for 30' at 4°C.

6. Immunohistochemical analysis

Immunohistochemical staining was performed on formalin-fixed, paraffin-embedded (FFPE) tissues using a standard avidin-biotin immunoperoxidase complex technique (Dako). Briefly, four-μm thick sections were mounted on silanized slides, dewaxed in xylene, dehydrated in ethanol, boiled in 0.01 M citrate buffer (pH 6.0) for 15 min in a microwave at 95 °C, and incubated with 3% hydrogen peroxide for 5 min. After washing with PBS, sections were incubated in PBS containing 10% BSA

for 30 min, followed by incubation for 45 min at room temperature with monoclonal (mAb) mouse anti-human cytokeratin 20 (CK20, 1:200; Abcam) or cytokeratin 18 (CK18, 1:100; Dako). The incubation with rabbit anti-human Msi-1 (1:100; Abcam) and mouse anti-human Lgr5 (1:200; Origene), was performed overnight at 4°C. After washings, the sections were incubated with biotinylated goat anti-mouse immunoglobulin (LSAB kit, Dako) or anti-rabbit immunoglobulin (Vectastain ABC kit, Vector Lab, Burlingame, CA) and peroxidase-conjugated avidin (Dako). Lastly, 0.02% diaminobenzidine and 1% hydrogen peroxide (Dako) in PBS were used as substrates in the color development reaction. Sections were then counterstained with hematoxylin.

7. Immunocytochemistry

PKH26-labeled cells obtained by dissociation of the spheroid structures and sorted samples (FACS ARIA II, BD Biosciences) were seeded onto poly-D-lysine-coated glasses at $5x10^4$ cells/spot; MICOL-14^{tum} cells were instead made growth on multiwell chamber. Cells were fixed in 4% paraformaldehyde, followed by permeabilization with 0.1% Triton X-100 in PBS. Non-specific binding was prevented by saturation with PBS/5% BSA for 30 minutes. The cells were then incubated with the following anti-human mAb: Msi-1 (1:100; Abcam), Lgr5 (1:200; Origene), CK20 (Ks 20.8, 1:10; Dako), CK18 (1:200; Abcam), Mucin-1 (Muc-1, 1:100; Abcam) and Notch1 activated domain (N1ICD, 1:800, Abcam). For non-conjugated antibodies, secondary Alexa Fluor 488-conjugated goat anti-rabbit and Alexa Fluor 633-conjugated goat anti-mouse or Alexa Fluor 546-conjugated goat anti-mouse antibodies (1:500; Molecular Probes, Invitrogen) were added for 30 minutes. Glasses were finally washed twice with PBS and mounted in glycerol. Where possible nuclei were stained with Topro3 (1:1000, Molecular Probes, Invitrogen). Confocal laser scanning microscopy was carried out with a Zeiss LSM 510 microscope (Zeiss, Jena, Germany) using Argon (488nm) and Helium-Neon (543-633nm) laser sources.

8. Immunofluorescence analysis on frozen sections

Immunofluorescence was performed on frozen human colon mucosa samples. Briefly, 7-µm thick sections were collected on Superfrost Plus microscope slides (Thermo Scientific, Munich, Germany) and dried at room temperature for 20 min. Sections were fixed in 4% paraformaldehyde and permeabilized with 0.1% Triton X-100. Non-specific binding was prevented by incubation in PBS/5% BSA for 1 h. Staining was carried out by incubating the sections with the anti-Msi-1 (1:100; Abcam) and anti-CK20 (9:50; Dako) antibodies for 30 minutes at room temperature. After three washes in PBS, appropriate secondary Alexa-conjugated antibodies (1:500; Molecular Probes, Invitrogen) were added for 1h. Nuclear staining was performed by propidium iodide (PI) incubation (1:10.000; Invitrogen) and pictures acquired with confocal Zeiss LSM 510 microscope at 20x and 40x magnification.

9. RNA extraction, reverse transcription and quantitative Real-Time PCR (qRT-PCR) assay

Total RNA was extracted from different cell populations, spheroids, *in vitro* differentiated cells, and microdissected samples by the TRIzol method, according to the manufacturer's instructions. cDNA was synthesized from 0.5-1 µg of total RNA using the Superscript II reverse transcriptase (Invitrogen). Fifty-five ng of cDNA were used as a template and mixed with 10 µl of 2X Platinum SYBR Green qPCR SuperMix-UDG (Invitrogen) and primers, listed in Table 3, in a reaction volume of 20 µl. Cycling conditions were 10 min at 95°C, 60 cycles of 15 s at 95°C and 1 min at 60°C. Each sample was run in duplicate on ABI PRISM® 7900HT Sequence Detection System (PE Biosystems, Foster City, CA). Results were analyzed using the comparative ΔΔCt method: data are presented as the fold difference in gene expression, normalized to the housekeeping gene β_2-microglobulin and relative to a relevant reference sample. qRT-PCR efficiency was always in the range 95-105%.

Gene name	Forward	Reverse
Lgr5	5’-CTCTTCCTCAAACCGTCTGC-3’	5’-GATCGGAGGCTAAGCAACTG-3’
Msi-1	5’-GGTTTCCAAGCCACAACCTA-3’	5’-TCGGGGAACTGGTAGGTGTA-3’
CK20	5’-GACGCCAGAACAACGAATACC-3’	5’-ACGACCTTGCCATCCACTAC-3’
β2Micro	5’-TCTCTCTTTCTGGCCTGGAG-3’	5’- TCTCTGCTGGATGACGTGAG-3’
Bmi-1	5’-GCATCGAACAACGAGAATCA-3’	5’-TACCCTCGACAAAGCACACA-3’
EpCAM	5’-CCAGAACAATGATGGGCTTT-3’	5’-GCACTGCTTGGCCTTAAAGA-3’
ALDH1	5’-CCCGTTGGTTATGCTCATTT-3’	5’-TGCTCTGCTGGTTTGACAAC-3’
Muc-1	5'-AGTTCAGGCCAGGATCTGTG-3'	5'-GAAATGGCACATCACTCACG-3'
Muc-2	5-'ACCCGCACTATGTCACCTTC-3'	5'-GGGATCGCAGTGGTAGTTGT-3'
EpHB2	5’-TCCATCTGGGACTTTCAAGG-3’	5’-TGTTGATGGGACAGTGGGTA-3’
Notch-1	5'-GTGCCCTCATGGACGACAAC-3'	5'-GCATCCAGGTGCTGCTGAGT-3'
Notch-2	5'-CAGCCTGTATGTGCCCTGTG-3'	5'-GTGCTCCCTTAAAACGTGCA-3'
Notch-3	5'-CAAGGGTGAGAGCCTGATGG-3'	5'-GAGTCCACTGACGGCAATCC-3'
Hes-1	5'-CAGCGGGCGCAGATGAC-3'	5'-CGTTCATGCACTCGCTGAAG-3'
Hey-2	5'-GGCGTCGGGATCGGATAAAT-3'	5'-GCGTGTGCGTCAAAGTAGCC-3'
Numb	5'-AGCCAGCCCATACTGCTCTA-3'	5'-CGGACGCTCTTAGACACCTC-3'

Table 3 **Sequences of the primers used in qRT-PCR experiments.**

10. Notch assay

To stimulate Notch signaling, P12 wells were coated with soluble recombinant human DLL4 (4 μg/ml) (R&D, Minneapolis, MN, USA) in PBS/BSA 0.1%. One day later, MICOL-14^{tum} or primary sample cells were added at a concentration of $2x10^5$ cells/well in RPMI-1640 medium supplemented with 10% FCS and 1% L-glutamine (Invitrogen) and cultivated for 72 h prior to subsequent analysis. The monoclonal antibodies, including α-Notch2/3 (OMP-59R5) and the control antibody (CTRL) (OMP-1B711), kindly provided by *OncoMed Pharmaceuticals Inc*, (Redwood City, CA) were used at 10 μg/ml final concentration.

11. Western Blotting

According to experimental design after 72 h of treatment, or after 3 weeks of culture, FACS-sorted PKH^{pos} cells, *in vitro* differentiated cells or cells treated with α-Notch2/3 antibody were harvested, lysed and subjected to SDS-polyacrylamide gel electrophoresis and Western Blotting (WB). The membrane was saturated with

PBS/5% non-fat dry milk (Sigma Aldrich) for 1 h at room temperature. Immunoreactivity was evaluated by hybridization using the following antibodies: rabbit anti-Msi-1 (1:1000; Abcam), mouse anti-Muc-1 (1:1000; Abcam), rabbit anti-Numb (1:500; Millipore, Billerica, MA, USA), rabbit anti Notch1 activated domain (N1ICD, 1:1000; Cell Signaling, Beverly, Massachusetts) and mouse anti- α tubulin (1:5000; Sigma Aldrich). The blots were then hybridized with a 1:5000 dilution of HRP-conjugated anti-mouse or anti-rabbit antibody (Amersham-Pharmacia, Little Chalfont, UK). Finally, the signal was detected by chemiluminescence with SuperSignal kit (Pierce, Rockford, IL).

12. Reporter gene assay

MICOL-14^{tum} cells were transiently co-transfected using lipofectamine 2000 (Invitrogen) with a CSL-luc plasmid, a Notch-responsive reporter construct carrying the luciferase reporter gene under the control of a promoter containing CSL binding sites [89], and a plasmid encoding β-galactosidase under the control of the human CMV promoter, which was used to normalize transfection efficiency. One day later, cells were split and cultivated for additional 48 h on wells coated with human DLL4 (4 μg/ml) or BSA, as control. Each experiment was repeated at least three times. Cell lysates were harvested 72 h post-transfection and luciferase and β-galactosidase assays were carried out using BriteLite Plus (Perkin-Elmer, Waltham, Massachusetts) and Tropix® Galacto-Light™ (Applied Biosystems), respectively, on a plate luminometer (Perkin-Elmer).

13. Transduction of cells with viral vectors

Lentiviral vectors encoding shRNA targeting human Notch3 or a scrambled shRNA as control were purchased from Sigma-Aldrich and used as previously reported [83]. The CEG-N3 retroviral vectors, encoding constitutively active forms of human Notch3 and the control CEG vector have been described in detail elsewhere [90]. The Notch2 ICD encoding retroviral vector (pMSVpuroICN2) was a gift from Adolfo Ferrando (Columbia University, NY). The human DLL4-EGFP and the control retroviral construct lacking DLL4 have been previously described

[91]. Vector stocks were generated by a transient three-plasmid vector packaging system, as previously described [92]. For transduction of MICOL-14^{tum} cells, 200 µL of concentrated vector-containing supernatant were layered over target cells that had been seeded into 12-well culture plates at 1×10^5 cell/well. After 6 to 9 h at 37°C, the supernatant was replaced with 2 mL of complete medium. Assessment of transgene expression was performed 72-96 h after transduction.

14. Cells Isolation by Laser Microdissection

Snap-frozen colon biopsies were embedded in cryostat embedding medium (Bio Optica, Milan, Italy), cut into serial 7-µm sections and collected onto PEN-membrane slides (Leica, Wetzlar, Germany). Sections were fixed in 70% ethanol followed by nuclear staining with hematoxylin and dehydration in alcohol. Only longitudinally cut crypts were considered for microdissection. Three cell populations were isolated: putative stem-like cells at the very crypt base (2-3 cells/crypt), Transient-Amplifying (TA) cells located along the crypt wall, and terminally differentiated cells at the crypt apex and mucosal surface. Each population was isolated by a laser microdissection system (Leica DM6000 B), and collected on the test tube cap. For each population at least $1x10^4$ cells were collected in the appropriate amount of TRIzol (Invitrogen), and kept at -80°C until RNA extraction.

15. Tumorigenicity assay

NOD/SCID mice were purchased from Charles River (Wilmington, MA, USA). Procedures involving animals, and their care, were performed according to institutional guidelines that comply with national and international laws and policies (EEC Council Directive 86/609, OJ L358, 12 December 1987). For tumor establishment, MICOL-14^{tum} cells were washed and resuspended in PBS. Seven- to nine-week-old male mice were injected subcutaneously with $5x10^5$ cells in a 200 µl total volume in both dorsolateral flanks. At the tumors establishment, mice were sacrificed by cervical dislocation; tumors were harvested by dissection, fixed in formalin and embedded in paraffin (FFPE) for immunohistochemical analysis.

16. Statistical Analysis

Data of replicate experiments were shown as mean value ± Standard Deviation (SD). Comparisons between groups were made by the Student's t-test.

RESULTS

1. NORMAL COLON STEM CELLS

1.1 Identification of a slowly cycling cell population and in vitro spheroid formation

Following isolation from fresh normal colon mucosa samples, the cells were stained *in vitro* with PKH26, a dye which binds membrane phospholipids, thus conferring a bright red fluorescence [86]. PKH26 staining may represent an unconventional proliferative assay and a surrogate marker of stemness, akin DNA labels such as Bromodeoxyuridine (BrdU). In fact, the dye segregates during each cell division, and a progressive decrease of fluorescence intensity in daughter cells can be observed [93], allowing to monitor by FACS the cells which proliferate more slowly based on their brighter appearance. Immediately after staining, >98% of the cells were PKH^{pos} (Fig. 11A); in the subsequent weeks, a progressive increase in the number of cells expressing the dye at low intensity (PKH^{low}) was observed, until virtually only cells with high PKH26 expression (PKH^{high}) remained (Fig. 11A), indicating that the cultures contained cells with different replicative potential.

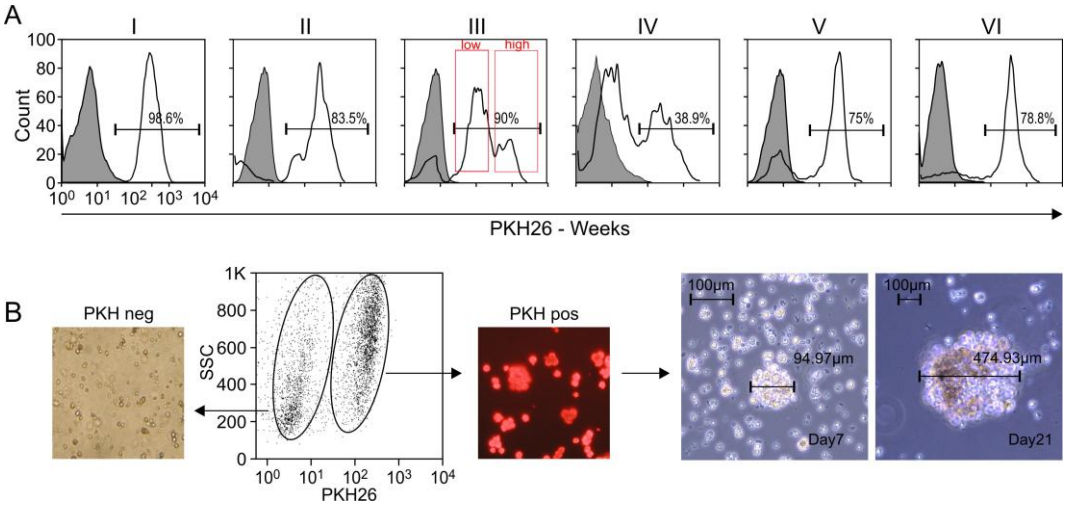

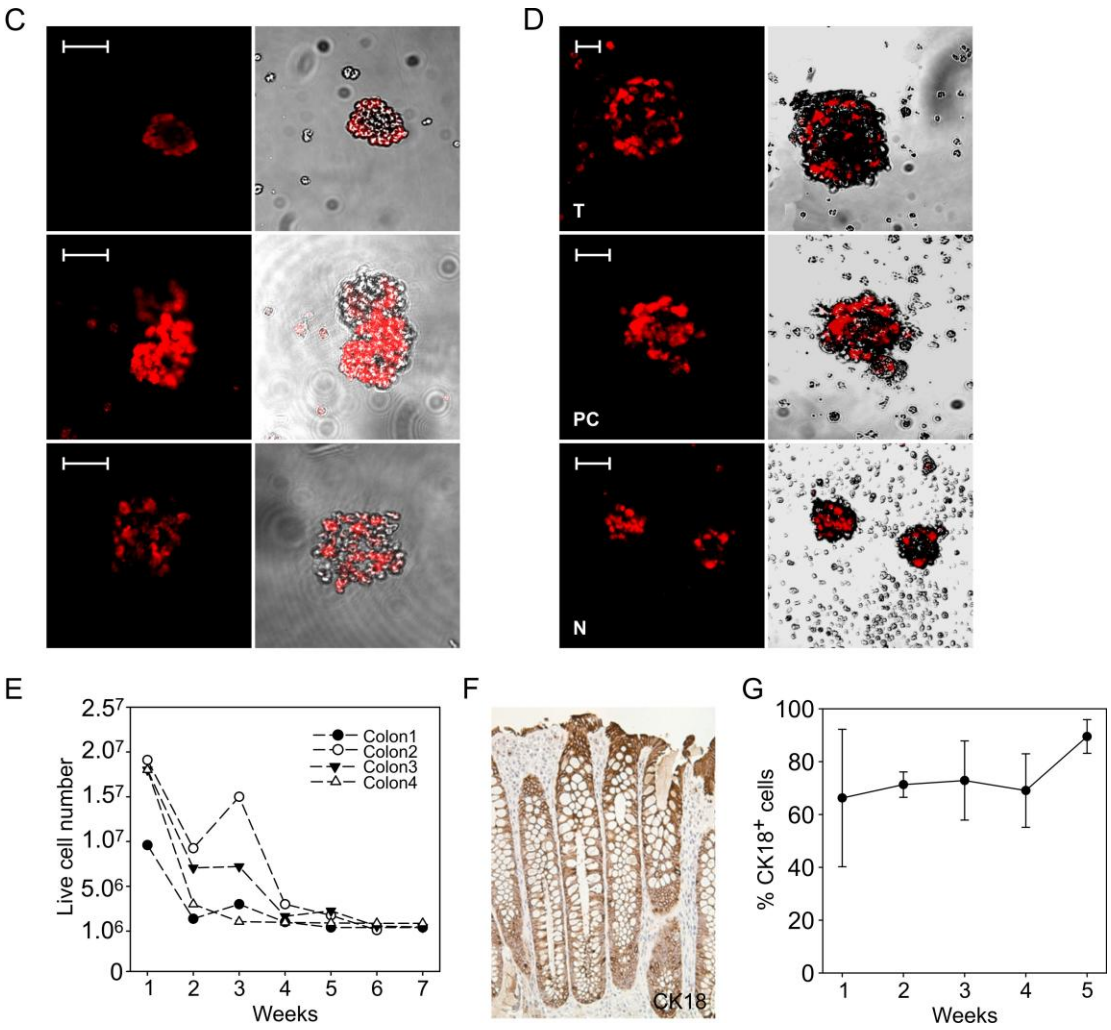

Figure 11. **Kinetics of PKH26 and *in vitro* spheroid formation.**
(A) Cells obtained from human normal colon samples were cultured *in vitro* as detailed in *Materials and Methods*, and stained with PKH26. Cytofluorimetric analysis of PKH staining over 6 weeks of culture showed the progressive selection of a cell population expressing the dye at high intensity. At the 3rd week of culture, within the PKH^{pos} subset it was possible to distinguish two major peaks (PKH^{high} and PKH^{low}). One representative experiment is shown. (B) Three weeks after PKH26 staining, PKH^{pos} and PKH^{neg} cells were FACS-sorted and cultured under serum-free conditions as detailed in *Materials and Methods*. While PKH^{neg} cells rapidly died in culture (left panel), PKH^{pos} cells began to form spheroid-like structures, which progressively grew over time in culture (right panels; magnification 20x, scale bars: 100μm). (C) Confocal microscopy analysis of spheroids showed cells with different intensity of PKH26 staining at 3 weeks of culture; magnification 20x. (D) Spheroids obtained after 3-week culture from PKH^{pos} cells isolated from tumor [T] and pre-cancerous [PC] human colon samples were morphologically comparable to those obtained from normal [N] colon tissue. Scale bars: 100 μm. (E) Kinetics of cell survival in culture; in the absence of serum, the number of living cells decreased until about 5% of input cells at the end of the culture period. Results obtained in 4 consecutive experiments are shown. (F) CK18 staining of a human colon mucosa section (10x magnification). (G) Kinetics of CK18 expression in cultured colon cells; data are expressed as mean values ± SD of six different experiments.

Several studies have demonstrated that under specific culture conditions one of the major properties of cancer stem cells is their ability to form spheroids *in vitro* [94-

95]. When PKH^{pos} and PKH^{neg} cells were FACS-sorted at the 3rd week after PKH staining, and cultured in the absence of serum as detailed in *Materials and Methods*, within a few days PKH^{pos} cells began to form small, round cell clusters which grew into spheroid structures (Fig. 11B), whereas sorted PKH^{neg} cells died within 2-6 days, and no spheroid-like structures could be observed. Confocal microscopy analysis revealed that these spheroids contained a heterogeneous mixture of cells with different PKH26 staining intensity and cells negative for the dye, often spatially segregated within a same structure (Fig. 11C). By a limiting dilution assay, in three consecutive experiments the frequency of spheroid-forming cells was ranged for 1/100 to 1/220 PKH^{pos} cells, whereas, as expected, this frequency was much lower when unfractionated epithelial cells were plated (Table 4).

Number of cells/well	**Number of wells plated**	**Number of wells showing spheroids**	
		Unfractionated cells	**PKH^{+} cells**
10,000	30	30	30
2,000	30	18	30
400	30	9	26
80	30	2	16
16	30	0	12
3	30	0	5
Spheoids forming frequency		1/1,748	1/107

Table 4. **Extreme limiting dilution analysis of spheroid-forming cell precursors in normal colon epithelial cell populations.** P-value <0.0001; Data were pooled from three independent experiments.

Microscopic evaluation showed that spheroids obtained from purified PKH^{pos} cells from normal colon mucosa were fully comparable to those obtained from PKH^{pos} cells isolated by the same technique from colon tumors and pre-cancerous lesions after 3 weeks of culture (Fig. 11D).

On the other hand, the surviving PKH^{pos} subset was a minority of the original population, as the total number of cells in culture decreased over time, and by 6 weeks only about 5% of the cells originally present at the beginning of the culture

could be recovered (Fig. 11E). Flow cytometry analysis for CK18, a known marker of colon epithelium (Fig. 11F), revealed that early in culture the majority of the cells also expressed CK18 (Fig. 11G); this percentage increased over time, with >95% of the surviving cells positive for both PKH26 and CK18 by 5 weeks of culture (Fig. 11G). Altogether, the above results pointed to the existence, within epithelial colon cells, of a slowly dividing subset able to maintain PKH26 staining *in vitro*, which could be a suitable candidate for a stem cell-containing population.

1.2 Stemness marker expression by in vitro cultured colon cells

To characterize the cell population responsible for spheroid generation, we analyzed the expression of two putative markers of colon stem-like cells, Msi-1 [30] and Lgr5 [96, 97]. As judged by immunohistochemistry on colon biopsies, Msi-1 staining was substantially confined to the crypt basement (Fig. 12A, left panel), where colon stem cells are expected to reside [98], while the paucity of Lgr5-stained cells at the very crypt bottom (Fig. 12A, right panel) fully confirmed previous data [47]. As demonstrated by three-color cytofluorimetry at the 3rd week of culture, Msi-1^{+} cells were mainly confined within the slowly cycling PKH^{high} cell population, but a sizable fraction of PKH^{low} cells also expressed this marker, whereas no Msi-1 expression could be detected in PKH^{neg} cells (Fig. 12B, middle panel). Lgr5 expression, instead, was entirely restricted to PKH^{high} cells, and no Lgr5 expression was recorded in epithelial cells showing lower PKH26 levels (Fig. 12B, lower panel).

Flow cytometry analysis revealed that the percentage of Msi-1^{+} and Lgr5^{+} cells increased over the culture period (Fig. 12C); at the 4th week of culture 28.7 ± 2.4% of the PKH^{high} cells expressed the Msi-1 antigen, while 24.9 ± 3.6% expressed Lgr5, thus indicating an enrichment of Msi-1^{+} and Lgr5^{+} cells in the PKH^{high} population. As shown in Figure 12D, at all times of culture Lgr5^{+} cells invariably co-expressed Msi-1, and this subset consistently augmented over the culture period, while a small population of Msi-1^{+} cells that did not express Lgr5 was found, which underwent progressive reduction late in culture (Fig. 12D).

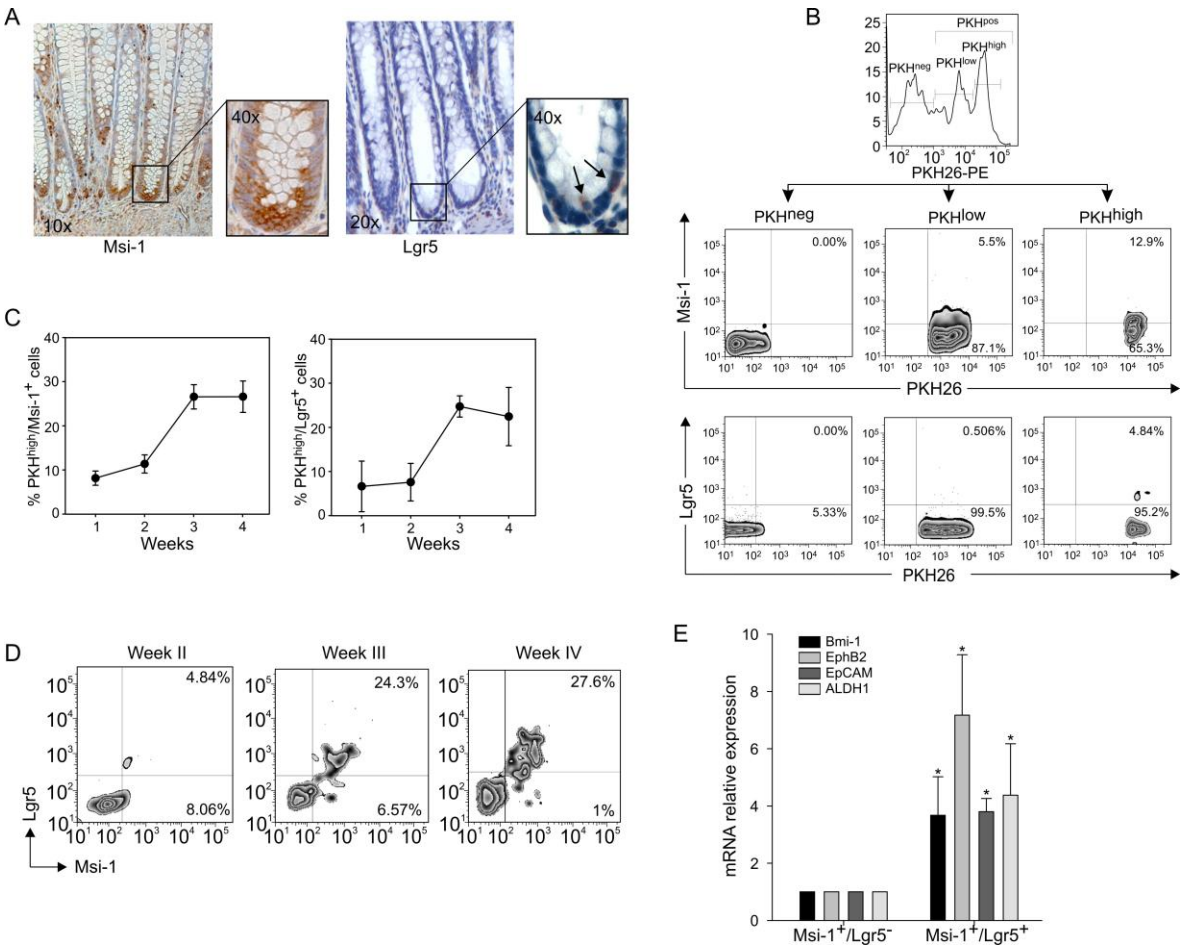

Figure 12. **Expression of stemness-associated markers in cultured colon cells.**
(A) Immunohistochemical analysis of Msi-1 and Lgr5 expression in human normal colon biopsies; Msi-1^+ and $Lgr5^+$ cells are localized at the crypt base, where *bona fide* stem-like cells home; magnification is indicated in the boxes. (B) Cytofluorimetric analysis of Msi-1 and Lgr5 expression by PKH26-labelled cells expressing different intensities of PKH26 staining (PKH^{neg}, PKH^{low} and PKH^{high}; upper panel) at the 3rd week of culture. Msi-1^+ cells were found within both PKH^{high} and PKH^{low} cell populations (middle panels), whereas $Lgr5^+$ cells were confined to the PKH^{high} subset (lower panels). One representative experiment out of three consecutive is shown. (C) Cytofluorimetric analysis of Msi-1 and Lgr5 expression by PKH^{high} cells over 4 weeks of culture. Data are expressed as percent mean values (± SD) of 5 consecutive experiments. (D) Kinetics of Msi-1 and Lgr5 expression by PKH^{high} cells at the 2nd, 3rd and 4th week of culture. All $Lgr5^+$ cells also co-expressed Msi-1, whereas a small fraction of Msi-1^+ cells did not express Lgr5. One representative experiment out of 4 is shown. (E) qRT-PCR analysis of expression of Bmi-1, EphB2, EpCAM and ALDH1 in FACS-isolated Msi-1^+/$Lgr5^-$ and Msi-1^+/$Lgr5^+$ cell subsets at the 3rd week of culture. Data were calculated as mean values ± SD as detailed in *Materials and Methods*, normalized to the housekeeping gene β_2-microglobulin and relative to the reference sample (Msi-1^+/$Lgr5^-$ cells). * $p<0.05$.

We also compared in FACS-purified Msi-1^+/$Lgr5^-$ and Msi-1^+/$Lgr5^+$ cells the expression of other putative markers for colon stem cells, such as Bmi-1 [99], EphB2

[100], EpCAM [45], and ALDH1 [101]. qRT-PCR analysis of FACS-sorted cells after 3 weeks of culture revealed that the mRNA expression levels of all these genes were consistently higher ($p<0.05$) in Msi-1^+/Lgr5^+ than in Msi-1^+/Lgr5^- cells (Fig. 12E). Thus, these findings seemed to indicate that the Msi-1^+/Lgr5^+ cell population is strongly enriched in stem-like cells, compared to Msi-1^+/Lgr5^- cells. Altogether, the above data seemed also to delineate the existence of a sort of stemness "gradient" in the cultured population, where at least 3 discrete cell subsets could be identified, a PKH^{high}/Lgr5^+/Msi-1^+ population (reasonably reflecting relatively quiescent cells endowed with most prominent stem-like properties), a PKH^{high}/Lgr5^-/Msi-1^+ subset (likely reflecting cells with a slow division rate, which lost the expression of a key stemness marker such as Lgr5), and a PKH^{low}/Lgr5^-/Msi-1^+ population which had likely undergone more cycles of replication.

1.3 Stemness and differentiation marker co-expression by in vitro cultured cells

CK20 is considered as a marker of differentiated intestinal epithelial cells [47]; a preliminary confirmation of the ability of anti-CK20 antibody to identify differentiated epithelial cells was obtained by immunohistochemistry in colon sections (Fig. 13A). CK20 expression was mostly confined, as expected, to PKH^{neg} cells (Fig. 13B), which reasonably underwent more cycles of replication. Surprisingly, although the vast majority of CK20^+ cells did not express Msi-1 (Fig. 13B), double staining with anti-Msi-1 and anti-CK20 antibodies of cells cultured for 3 weeks revealed the presence of a small population expressing both markers only in the PKH^{high} subset (Fig. 13B). In 4 consecutive experiments, Msi-1^+/CK20^+ cells accounted for $5.13 \pm 0.32\%$ of this most brilliant population. No co-expression of Lgr5 and CK20 was observed (not shown), and the Msi-1^+/CK20^+ population was virtually absent in the PKH^{low} subset. The presence of a small population expressing both Msi-1 and CK20 was also supported by confocal microscopy analysis of cells cultured for 3 weeks (Fig. 13C).

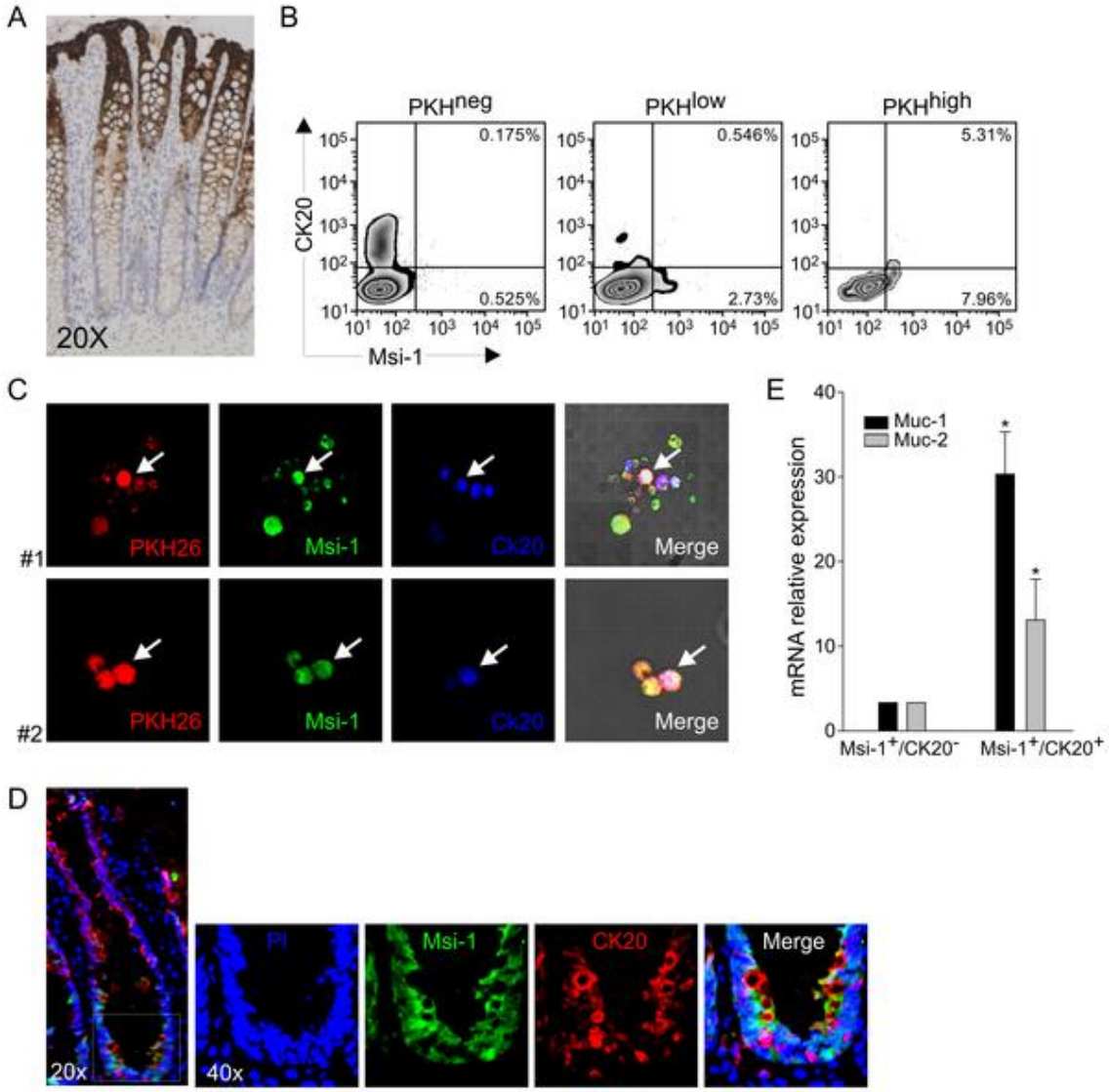

Figure 13. **Expression of Msi-1 and CK20 in cultured colon cells**
(A) Immunohistochemical analysis of CK20 showed labeling of the epithelial cells along the crypt wall and at the mucosal surface, but not at the crypt bottom. (B) Cytofluorimetric analysis of Msi-1 and CK20 expression by PKH^{neg}, PKH^{low} and PKH^{high} populations at the 3rd week of culture; a small subset of PKH^{high} cells co-expressed both markers. One representative experiment out of 4 consecutive is shown. (C) Confocal microscopy analysis of CK20 and Msi-1 expression in PKH^{pos} cells. The cells co-expressing both markers are indicated by an arrow. Magnification 40x. (D) Immunofluorescence analysis of Msi-1 and CK20 expression in frozen colon sections. Double-positive cells are evident at the very crypt base. (E) qRT-PCR analysis of Muc-1 and Muc-2 expression on FACS-sorted $Msi\text{-}1^{+}/CK20^{-}$ and $Msi\text{-}1^{+}/CK20^{+}$ subsets at the 3rd week of culture. Data are calculated as mean values ± SD as detailed in *Materials and Methods*, normalized to the housekeeping gene β_2-microglobulin and relative to the reference sample ($Msi\text{-}1^{+}/CK20^{-}$ cells). *$p<0.05$.

In view of the possible artefactual nature of these findings, we addressed the presence of these double-positive cells in colon crypt sections. As shown in Figure 13 D, the *in vivo* presence of $Msi\text{-}1^{+}/CK20^{+}$ cells could be demonstrated by

immunofluorescence analysis of frozen colon sections. This observation confirms previous data by Dalerba *et al*. [102], who identified $CK20^+$ goblet cells in close proximity to the more immature cellular compartment of the crypt bottom. Indeed, quantitative PCR analysis of FACS-sorted Msi-1^+/$CK20^+$ and Msi-1^+/$CK20^-$ cells at the 3rd week of culture revealed a significantly higher expression of Muc-1/2 in the double-positive subset (Fig. 13E).

1.4 Molecular analysis of in vitro cultured cells and microdissected colon crypt populations

The expression of genes putatively reflecting different stemness and differentiation stages was also compared by qRT-PCR in PKH^{high}, PKH^{low} and PKH^{neg} cells sorted after 3 weeks of culture, and in cells isolated from different colon crypt portions by microdissection. PKH^{high} cells showed significantly higher ($p<0.05$) mRNA levels of both Msi-1 and Lgr-5, as compared to PKH^{low} cells, while no expression of these genes was detected in the PKH^{neg} subset (Fig. 14A). As expected, opposite results were obtained for CK20 mRNA levels, which were significantly higher in the PKH^{neg} and PKH^{low} cell subset (Fig. 14A). By taking advantage of the discrete location of the cells within the colon mucosa, the above results were compared to mRNA levels of the same genes in three colon cell populations isolated through laser microdissection (Fig. 14B): cells at the very crypt bottom (which *bona fide* include Crypt Basal Columnar, CBC, cells and would correspond to cultured PKH^{high} cells), TA cells along the crypt wall (which are reasonably representative of cultured PKH^{low} cells) and terminally differentiated cells at the crypt apex and mucosal surface (likely reflecting PKH^{neg} cells). As expected, Msi-1 and Lgr-5 mRNA levels were much higher in the basal crypt cell population, and barely or not detectable at all in terminally differentiated cells (Fig. 14C). Thus, these data further buttressed the idea that the *in vitro* derived PKH^{high} population could indeed contain colon cells endowed with stem-like properties.

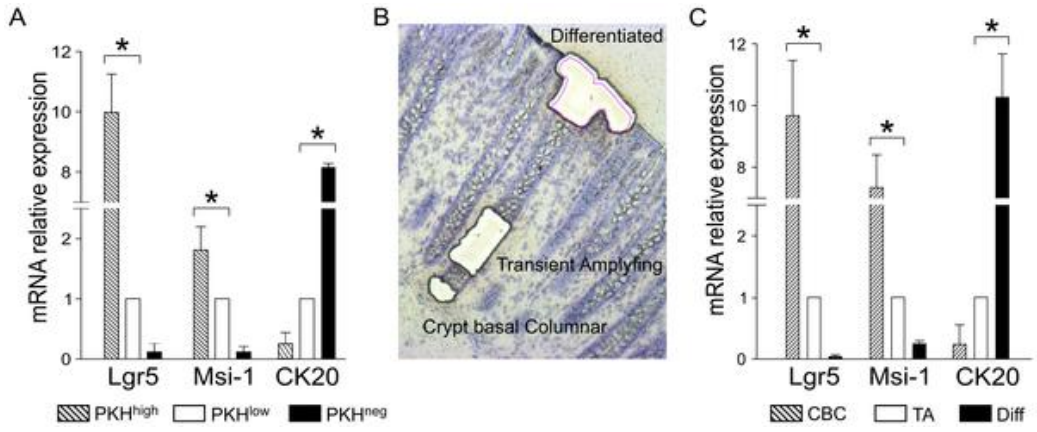

Figure 14. **Comparison by qRT-PCR of stemness and differentiation marker expression in cultured colon cells and microdissected colon crypt populations.**
mRNA levels of Lgr5, Msi-1 and CK20 genes were evaluated by qRT-PCR on FACS-sorted PKH^{high}, PKH^{low} and PKH^{neg} cells at the 3rd week of culture (Panel A) and on Differentiated (Diff), TA and CBC cells (Panel C) isolated by laser microdissection from colon crypts (as shown by the picture reported in Panel B). Data are shown as mean values ± SD calculated as described in detail in *Materials and Methods*, normalized to the housekeeping gene β_2-microglobulin and relative to the reference sample (PKH^{low} for sorted cultured cells, and TA for cells isolated by microdissection). * $p<0.05$.

1.5 In Vitro differentiation of cultured colon cells

To evaluate the differentiation potential of PKH26-stained cells, PKH^{pos} and PKH^{neg} subsets were sorted at the 3rd week of culture, and cultured in the presence of 10% FCS, in both uncoated and Matrigel-coated tissue culture plates. Under both culture conditions, PKH^{neg} cells died within 10 days (not shown), whereas PKH^{pos} cells survived but did not form spheroids, as they did in the absence of serum (Fig. 15A, upper panel). On the other hand, under differentiating conditions these cells showed a substantial proliferative potential and the ability to grow into organized structures; as shown by phase-contrast microscopy, in the presence of serum PKH^{pos} cells adhered to the plate assuming an epithelial morphology (Fig. 15A, middle panel), while in the presence of Matrigel, although not forming organoids similar to those recently described by Sato et al. [10], they generated branched structures of cells growing around "holes" (Fig. 15A, lower panel). Cytofluorimetric analysis revealed that the differentiated cells completely lost Msi-1 and Lgr5 expression just after 10 days of culture in serum and adhesion conditions (Fig. 15B). These data were also confirmed by WB analysis (Fig. 15C), which showed significantly higher

levels of Msi-1 protein in spheroids, compared to differentiated cells; these latter showed instead much higher levels of Muc-1 protein than cells grown under non-differentiating conditions (Fig. 15C). Furthermore, by comparing RNA extracted from both PKH^{pos} spheroid-forming cells and differentiated cells, we demonstrated an enrichment in the expression of the differentiation markers CK20, Muc-1 and Muc-2 ($p<0.05$) in PKH^{pos} cells maintained in adhesion condition and in the presence of serum for 10 days (Fig. 15D). Immunofluorescence analysis showed a partial loss of the PKH26 membrane labeling, which assumed a patchy pattern at the cells surface (Fig. 15E); furthermore, these cells expressed the differentiation markers Muc-1 (sample #1) and CK20 (sample #2), whereas Msi-1 expression was no longer detectable (Fig. 15E).

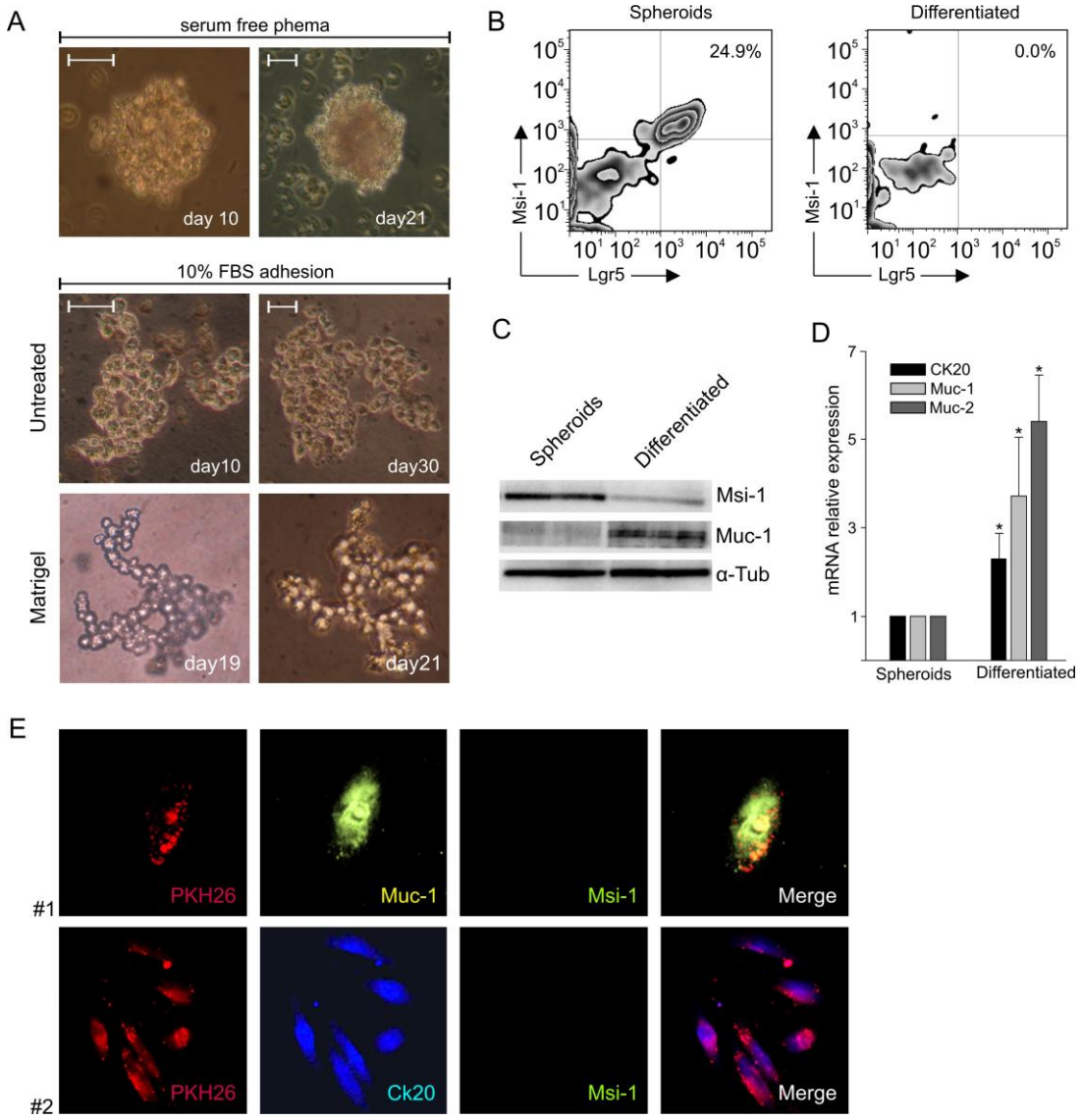

Figure 15. ***In vitro* differentiation of cultured PKH^{pos} cells.**
(A) After 3 weeks of culture the spheroids obtained from PKH-stained cells maintained in serum-free medium in non-adherent plates (upper panel) were dissociated, and PKH^{pos} cells were FACS-sorted and cultured in the presence of 10% FCS in adherent plates or included into Matrigel. In both conditions, the cells changed their morphology (lower panel), and in the presence of Matrigel they formed branched structures surrounding a "hole". (B) Cytofluorimetric analysis of Msi-1 and Lgr5 expression in PKH^{pos} cells cultured for 3 weeks in serum-free conditions (Spheroids) and after 10 days in differentiating conditions (Differentiated). (C) WB analysis of Msi-1 and Muc-1 proteins in Spheroids and Differentiated cell lysates. α-tubulin was used as a control for protein contents. (D) qRT-PCR analysis of CK20, Muc-1 and Muc-2 expression in Spheroids and Differentiated cells. Data are calculated as mean values ± SD as detailed in *Materials and Methods*, normalized to the housekeeping gene β_2-microglobulin and relative to the reference sample (spheroid cells). *$p<0.05$. (E) Confocal microscopy analysis of differentiated cells. In the presence of serum and adhesion conditions, the cells presented a fragmented PKH26 dye pattern along the cellular membrane, completely loosing the expression of Msi-1 while acquiring Muc-1 (sample # 1) and CK20 (samples #2) expression.

2. METASTATIC COLON CANCER STEM CELLS

2.1 Identification of a Slowly Cycling Cell Population and In Vitro Spheroid Formation

Once identified in normal samples a hierarchy of cell populations, we tried to describe their presence also in primary samples of colorectal cancer (CRC) and liver metastases from the same tumor. Thus we collected 5 primary CRC tumors and 15 metastatic samples, that were processed as described in *Material and Methods*. The cells were isolated, stained with PKH26, and cultured in PhEMA-treated plate in the absence of serum.

Flow cytometry analysis of PKH26 intensity revealed that, as the normal counterpart, in tumor samples after staining, more than 98% of the cells were PKH^{pos}; this percentage decreased during *in vitro* culture, until at the fourth week of culture mostly cells with high PKH26 expression remained (Fig. 16A) accounting for 70% of the total population. On the contrary, in the metastatic samples the PKH analysis did not definitely document an *in vitro* selection of a slowly cycling population (PKH^{high}). The percentage of PKH^{pos} cells decreased over the culture periods; the PKH^{high} subset progressively disappeared, until mostly PKH^{low} cells remained in culture, accounting for 65% of the total cell population at the fifth week (Fig. 16B). This event could reflect a continuous proliferation of metastatic cells even in the absence of serum, probably due to mutations accumulated during the neoplastic progression (Fig. 16C).

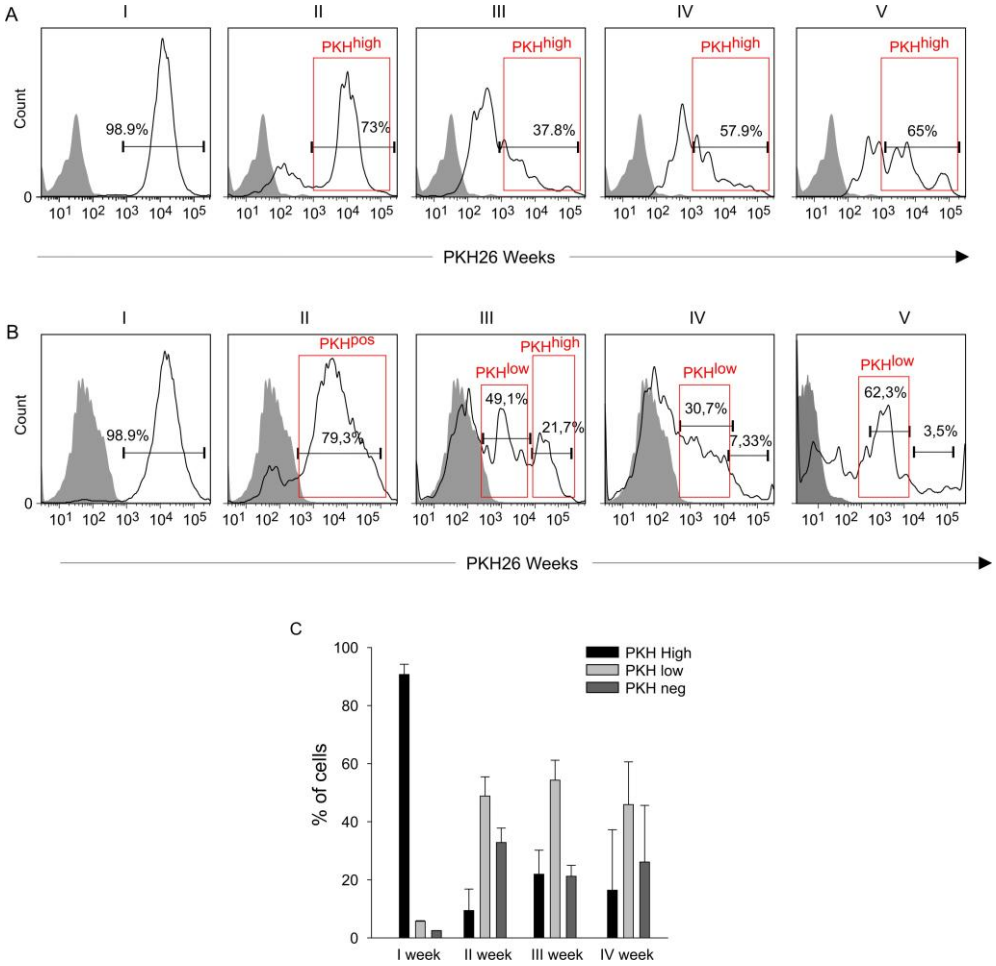

Figure 16. **PKH26 kinetic in tumor and metastatic samples.**
A) Cells obtained from human CRC samples were cultured *in vitro* as detailed in *Materials and Methods*, and stained with PKH26. Cytofluorimetric analysis of PKH stained cells over 5 weeks of culture showed the progressive selection of a cell population expressing the dye at high intensity, as in normal samples. One representative experiment is shown; B) Cells isolated from metastatic samples and stained with PKH26. Contrary to normal and tumor samples, cytofluorimetric analysis showed a selection of metastatic cells with an intermediate PKH intensity (PKH^{low}); one representative experiment is shown; C) Percentage of cells expressing the dye (PKH26) at different intensity: high, low and neg. Data, acquired by cytofluorimetryc analysis, are expressed as mean ±SD of six different experiments.

In metastatic samples we evaluated the cell ability to form spheroidal structures: PKH^{pos} cells (both PKH^{high} and PKH^{low}) were FACS-sorted from total population and cultured in PhEMA-treated plates. After 14 days, about 68% of samples were able to form spheroids that grew over time (Fig. 17A) independently from chemoterapic treatments of the patients (Table 5). Confocal microscopy analysis revealed that these spheroids, as well as those formed by normal samples, contained a heterogeneous mixture of cells with different PKH26 intensity (Fig. 17B).

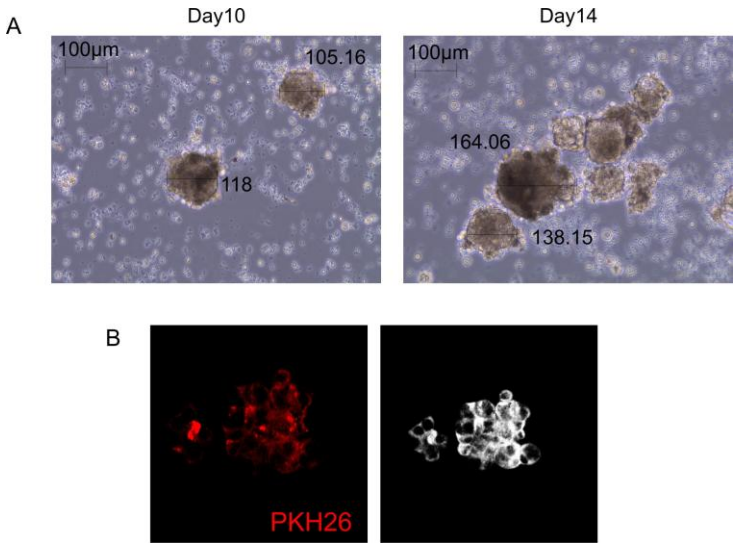

Figure 17. **Spheroid formation in metastatic CRC samples**
A) Sorted PKH^{pos} cells in PhEMA started to form spheroid-like structures that progressively grew over time in culture (magnification 20x, scale bar 100 µm); B) Confocal microscopy analysis of a spheroid obtained from sorted PKH^{pos} cells; cells with different intensity of PKH26 are present within the spheroidal structure (magnification 20x).

Sample ID	Treatment	Spheroids
HM#1	Folfiri	Yes
HM#2	no ct neoadiuvant	Yes
HM#3	Folfox	No
HM#4	Folfiri+Bevacizumab	Yes
HM#5	no ct neoadiuvant	No
HM#6	5Fu + Oxaliplatino	yes
HM#7	Folfiri + Bevacizumab	yes
HM#8	Folfiri + Bevacizumab	yes
HM#9	no ct neoadiuvant	no
HM#10	Folfox	yes
HM#11	Folfiri	yes
HM#12	Xelox	no
HM#13	no ct neoadiuvant	yes
HM#14	Xelodia	yes
HM#15	no ct neoadiuvant	no

Table 5. **Metastatic CRC samples**
The table correlates each sample, and patient chemioterapic treatment, with cell spheroid formation capability.

2.2 Stemness marker expression in metastatic CRC samples

We decided to evaluate putative stemness marker expression in the metastatic samples. The expression of the two stemness markers Lgr5 and Msi-1 was evaluated by flow cytometry after one week in low adhesion condition and during cell maintenance in PhEMA-treated plate. As for the normal counterpart, *ex vivo*, was identify a subset co-expressing Lgr5 and Msi-1 (Fig. 18A) accounting for about 9.8 ±3.4% of the total population. By three-color cytofluorimetry, it appeared evident that double-positive Lgr5/Msi-1 cells were not completely confined within the slowly cycling PKH^{high} cell population, but a sizable fraction was also present in PKH^{low} cells, while no Lgr5 or Msi-1 expression was recorded in PKH^{neg} cells (Fig. 18B). Thus, interestingly, at variance with normal samples, Lgr5 is expressed not only by the slowly cycling PKH^{high} cells but also by the PKH^{low} subset. Marker distribution was evaluated in total cell population during *in vitro* culture in five different samples; results indicated an increase up to 49.8 ± 7.8% in $Lgr5^{+}$/$Msi\text{-}1^{+}$ cells within four weeks of culture (Fig. 18C).

On the other hand, by analyzing the expression of other recognized CRC stemness markers such as CD133 and CD44, the co-expression of Lgr5 and Msi-1 appeared a more specific feature for SC identification (Fig. 18D). In fact CD44, as well as CD133, seemed to be expressed not only by the population $Lgr5^{+}$/$Msi\text{-}1^{+}$ *in toto* but also by other cells in the sample; the percentage of $CD44^{+}$ or $CD133^{+}$ cells was higher than that of $Lgr5^{+}$/Msi^{+} cells.

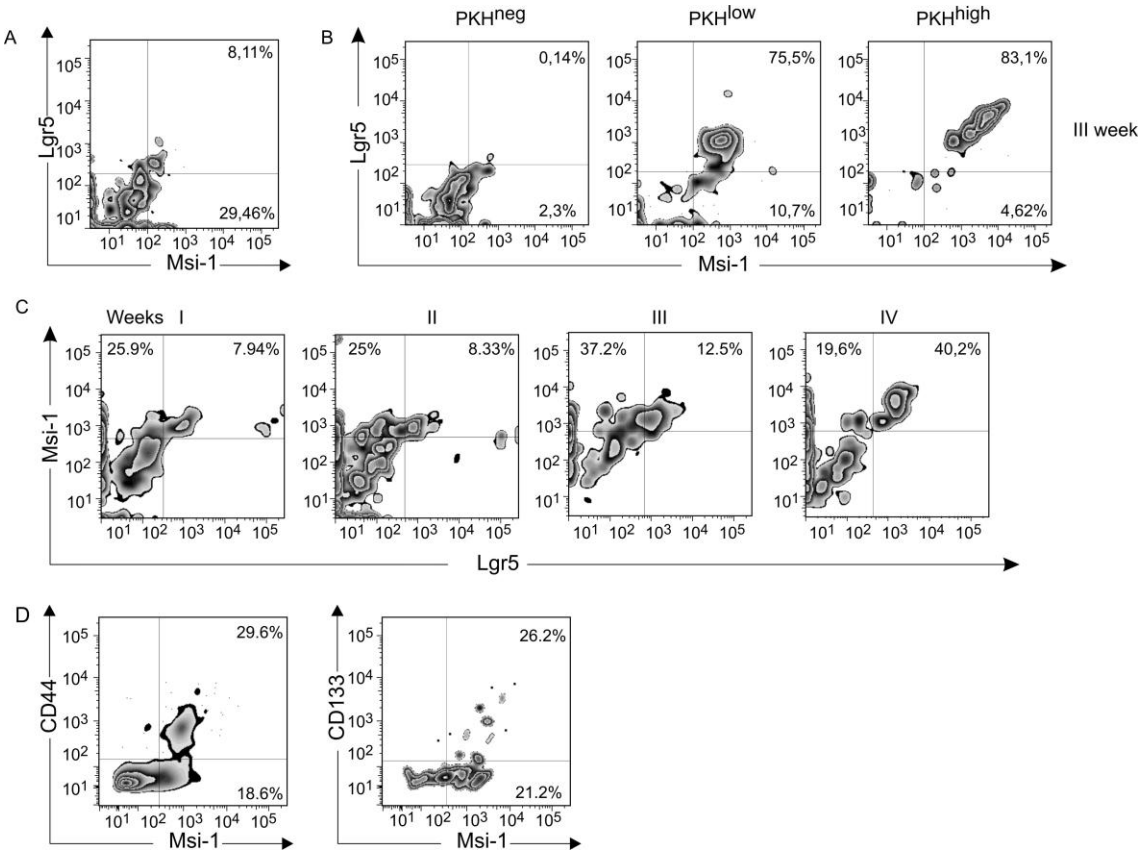

Figure 18. ***In vitro*** **stemness marker expression**
(A) Cytofluorimetric analysis of Msi-1 and Lgr5 expression by metastatic cells after one week in low adhesion condition; one representative experiment is shown; (B) Cytofluorimetric analysis of Msi-1 and Lgr5 expression by PKH26-labelled cells expressing different intensities of PKH26 (PKH^{neg}, PKH^{low} and PKH^{high}) at the 3rd week of culture. Msi-1^+/$Lgr5^+$ cells were found within both PKH^{high} and PKH^{low} cell populations, whereas no Msi-1^+/$Lgr5^+$ cells were detected in the PKH^{neg} subset. One representative experiment out of three consecutive is shown; (C) Kinetics of Msi-1 and Lgr5 expression by total cell population at the 1st, 2nd, 3rd and 4th week of culture. All $Lgr5^+$ cells also co-expressed Msi-1, whereas a small fraction of Msi-1^+ cells did not express Lgr5. One representative experiment out of 5 is shown; (D) Cytofluorimetric analysis of CD44, CD133 and Msi-1 expression by metastatic cells after one week in low adhesion condition; one representative experiment is shown.

Once identified within PKH^{pos} cells a subset expressing the stemness markers Lgr5 and Msi-1, we evaluated their differentiative potential. PKH^{pos} cells, sorted from spheroids, were cultured in the presence of 10% FCS in uncoated plates. After one week the cells did not form spheroids, as they did in the absence of serum; on the contrary, PKH^{pos} cells started to proliferate and adhere to the plate assuming an epithelial morphology, as shown by phase-contrast microscopy (Fig. 19A). Cytofluorimetric analysis revealed that these cells lost Msi-1 (not shown) and Lgr5

expression after 14 days of culture in the presence of serum (Fig. 19B) while they acquired the expression of CK20, a recognized marker of differentiation.

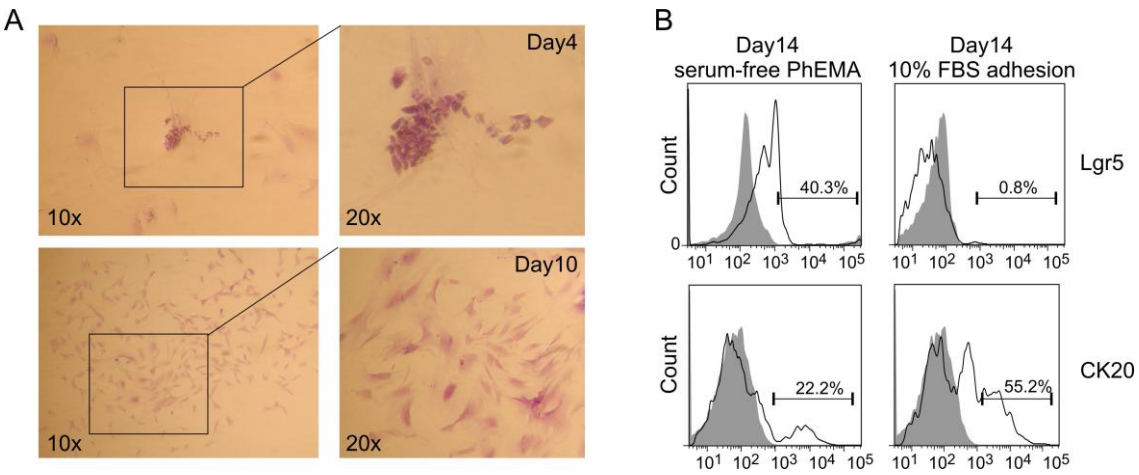

Figure 19. ***In vitro*** **Differentiation of Cultured PKH^{pos} Cells**
(A) Spheroids obtained from PKH^{pos} cells maintained in serum-free medium in non-adherent plates were dissociated, cells were FACS-sorted and PKH^{pos} cells were cultured in the presence of 10% FCS in adherent plates. The cells assumed an epithelial morphology as demonstrated by Crystal Violet staining; (B) Cytofluorimetric analysis of Lgr5 and Ck20 expression in PKH^{pos} cells after 2 weeks in serum-free condition (left panel) or in differentiation condition (right panel). One representative experiment out of three is shown; the grey colored peak in each histogram represents the istotype control and the empty black peak refers to stained cells.

3. MUSASHI-1 REGULATION BY THE NOTCH PATHWAY

3.1 DLL4 up-regulates Msi-1 transcript levels in CRC cells by a Notch2/3-mediated mechanism

Initially, we aimed at setting-up conditions for ligand-mediated stimulation of Notch signaling in CRC cells. To this end, MICOL-14^{tum} cells, transfected with a CSL-luc plasmid encoding the luciferase gene under the control of a Notch-responsive promoter, were stimulated by hDLL4. Seventy-two hours later, Notch activity was measured by in vitro luciferase assay. We observed an 8-fold increase in luciferase activity in hDLL4-stimulated cells, compared to basal levels (Fig. 20 A). Importantly, these effects were largely blocked by α-Notch2/3 but not α-Notch1 mAbs (Fig. 20A), suggesting that DLL4 stimulation triggers Notch signaling through Notch2 and/or Notch3 receptors in MICOL-14^{tum} cells, which express Notch1-3 but lack Notch4 [103]. These data were supported by measurement of endogenous components of the Notch pathway by qRT-PCR. Indeed, in 5 independent experiments, stimulation of MICOL-14^{tum} cells with hDLL4 significantly increased both Notch3 and Hey-2 transcript levels, and this effect was blocked by α-Notch2/3 mAb (Fig. 20B). Similar effects were also observed in primary cultures derived from CRC metastases (n=4). Indeed, Notch-3 and Hey-2 transcript levels were significantly increased after hDLL4 stimulation and markedly decreased in the presence of α-Notch2/3 (Fig. 20C). At variance with MICOL-14^{tum} cells, incubation of primary tumor cells with α-Notch2/3 significantly reduced levels of all Notch-related transcripts tested (including Notch1-3, Hey-1 and Hey-2) also in the absence of hDLL4 stimulation.

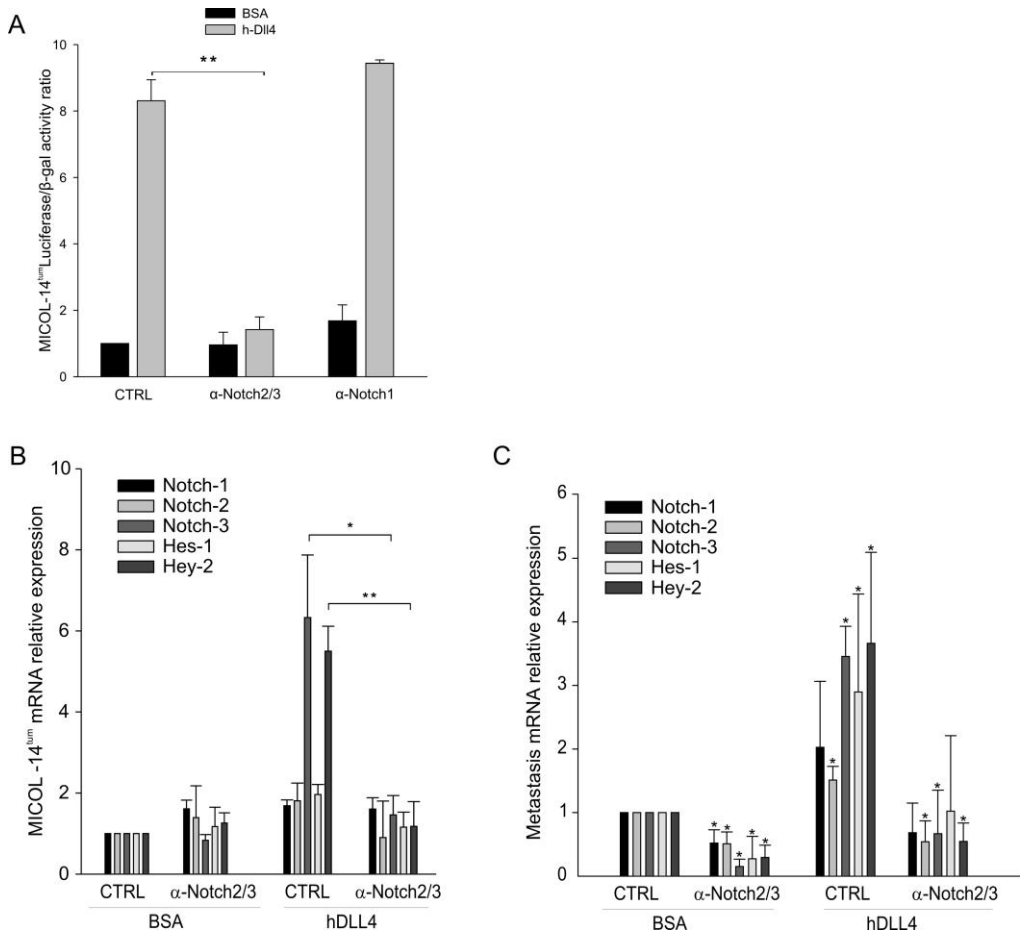

Figure 20. **Notch pathway modulation by Ab α-Notch2/3**
A) MICOL-14^{tum} cells transfected with the CSL-luc plasmid were stimulated for 72 h by recombinant human DLL4 (hDLL4). Notch activity was significantly blocked by α-Notch2/3 but not by α-Notch1. Data are expressed as mean ± SD of three independent experiments; B) Measurements by qRT-PCR of expression levels of Notch pathway components (Notch1-3, Hes-1, Hey-2) after 72 h of stimulation with hDLL4 in MICOL-14^{tum} cells. Data are expressed as mean ± SD of five different experiments; *p<0.05; C) Measurements by qRT-PCR of expression levels of Notch pathway components (Notch1-3, Hes-1, Hey-2) after 72 h of stimulation with hDLL4 in primary cultures from CRC liver metastases. Data are expressed as mean ± SD of four different experiments; *p<0.05.

Next, we investigated effects of DLL4 stimulation on the expression of stem cell-associated and differentiation markers. We observed that recombinant hDLL4 induced a 2-3-fold increase in Msi-1 levels in MICOL-14^{tum} cells, and this effect was largely blocked by α-Notch2/3 treatment. We also observed increased levels of Muc-1 mRNA following Notch2/3 blockade in all cultures analyzed (Fig. 21A). Since Muc-1 is a marker of colon epithelial cells differentiation, this finding could indicate that neutralization of Notch2/3 promotes cell differentiation. In contrast, only marginal changes in Muc-2 and Numb transcripts were detected in these experiments either in the presence or the absence of hDLL4 (Fig. 21A). Up-

regulation of Msi-1 levels was also observed following retroviral vector-mediated delivery of human DLL4 cDNA in MICOL-14^{tum} cells (Fig. 21B), thus confirming results obtained with recombinant hDLL4. To test whether the effect of hDLL4 was restricted to Msi-1 expression, we addressed the mRNA levels of several stem-associated genes in MICOL-14^{tum} cells after 72h of hDLL4 stimulation. As reported in Figure 21C, DLL4 stimulation significantly influenced Msi-1 expression, whereas Bmi-1, EpCAM and EpHB2 mRNA levels did not show any change, and ALDH expression only showed a marginal non significant increased.

HDLL4 induced a significant ($p<0.05$) increase of Msi-1 levels and a corresponding decrease in Muc-1 levels also in primary cultures derived from liver CRC metastases (Fig. 21D), and these modulations were completely blocked by α-Notch2/3. In primary tumor cultures, α-Notch2/3 caused significant reduction of Msi-1 expression and concomitant increase of Muc-1 levels also in the absence of recombinant hDLL4 stimulation (Fig. 21D), probably reflecting higher endogenous levels of Notch signaling compared to MICOL-14^{tum} cells.

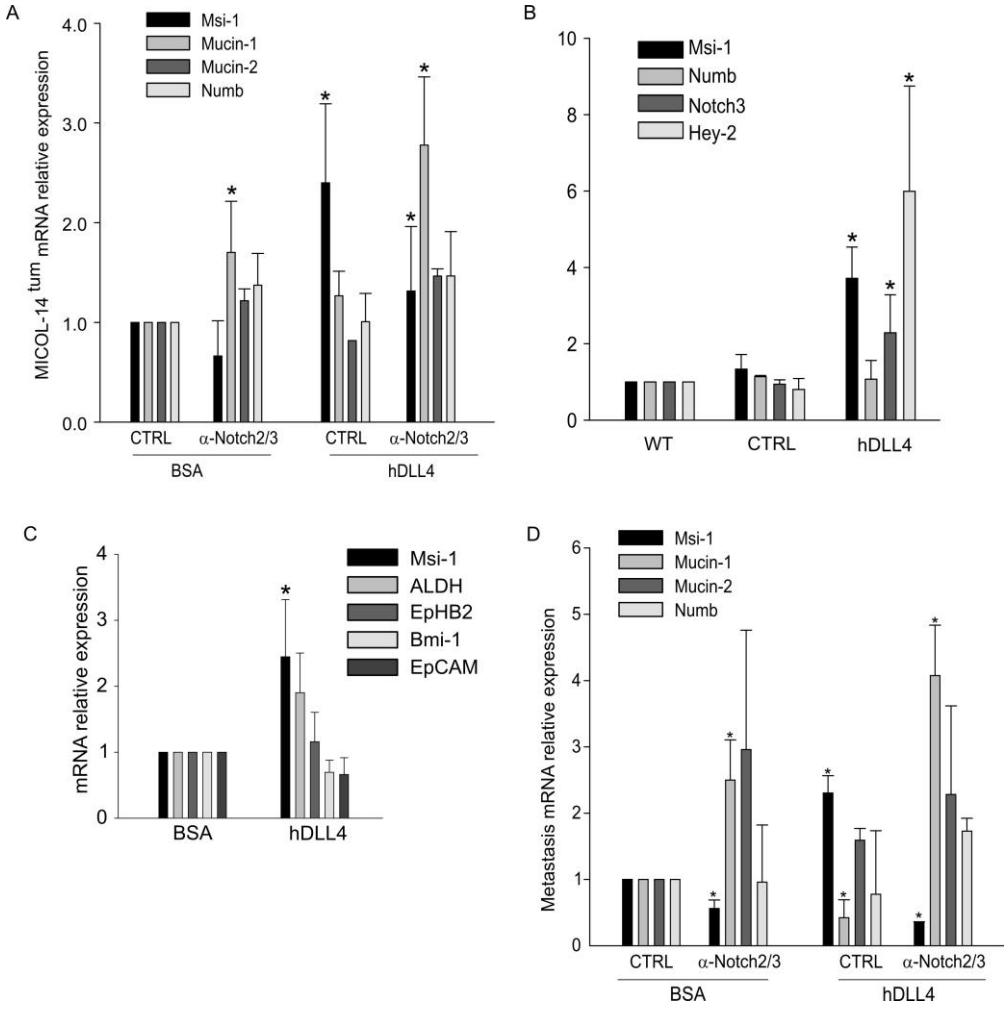

Figure 21**. DLL4-mediated increase of Msi-1 levels in CRC cells is blocked by α-Notch2/3 antibody**

A) qRT-PCR analysis of stemness-associated genes after 72h of stimulation with α-Notch2/3 or hDLL4 in MICOL-14^{tum} cells. Data are expressed as mean ± SD of five different experiments; *p<0.05; B) qRT-PCR after transfection of MICOL-14^{tum} cells with hDLL4 or the control vector (CTRL-EGFP). Msi-1, Notch3 as well as Hey-2 significantly increased while no alteration in Numb RNA levels were detected, comparing with control vector or no treated cells (wild type, WT). Data are expressed as mean mean ± SD of three different replicates; *p<0.05; C)qRT-PCR of stemness markers after 72h of stimulation with hDLL4 in MICOL-14^{tum} cells; Msi-1 is the only marker significantly increase after treatment; data are expressed as mean ± SD of four different experiments; *p<0.05; D) Measurements by qRT-PCR of stemness-associated genes after 72h of stimulation with α-Notch2/3 or hDLL4 in in primary cultures from CRC liver metastases. Data are expressed as mean ± SD of four different experiments; *p<0.05;

3.2 Effects of Notch2/3 blockade on Msi-1 and Numb levels in CRC cells

To validate these findings, we investigated the protein levels of Msi-1 in primary cultures of liver CRC metastases (n=5) by flow cytometry. Results indicated that hDLL4 increased until 18±4% Msi-1 expressing cells in tumor

samples. Moreover, α-Notch2/3 mAb strongly reduced (3.7±2.2%) the percentage of Msi-1^{+} cells both in hDLL4-stimulated and control cell cultures (Fig. 22A-B). Treatment with α-Notch1, conversely, had minimal effects on Msi-1 expression (Fig. 22A).

Immunofluorescence analysis confirmed that hDLL4 stimulation increased Msi-1 expression in MICOL-14^{tum} cells, and this effect was blocked by α-Notch2/3 mAb (Fig. 22C). In contrast, the expression levels of CK18, a common epithelial marker for colon cancer cells, were not affected by these treatments (Fig. 22C). Notably, α-Notch2/3 treatment markedly reduced Msi-1 protein levels also in the absence of hDLL4 stimulation (Fig. 22A-C), exceeding variations in Msi-1 transcript levels under the same experimental conditions (see Fig. 21A).

Finally, we analyzed reciprocal effects of hDLL4 stimulation and α-Notch2/3 blockade on Numb protein levels. We found that hDLL4 stimulation was associated with a small decrease in Numb protein levels and that α-Notch2/3 clearly increased Numb protein both in control and hDLL4-stimulated MICOL-14^{tum} and primary tumor cell cultures (Fig. 22D).

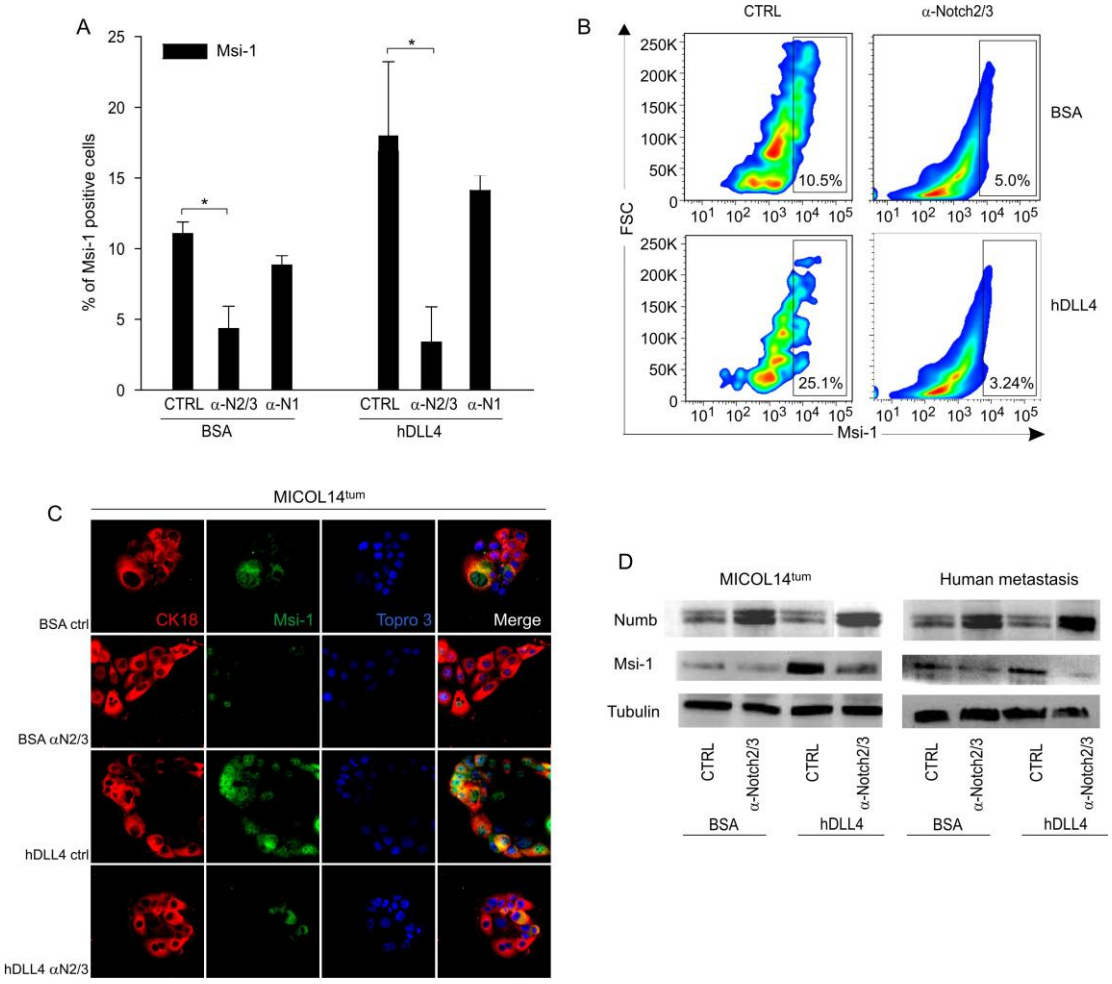

Figure 22. **Effects of hDLL4 and α-Notch2/3 on Msi-1 protein levels in CRC cells.**
A) Flow cytometry analysis of Msi-1 expression in primary cultures from liver CRC metastases cultivated for 72h in hDLL4-coated wells (or BSA as control) in the presence or the absence of α-Notch2/3, α-Notch1, or control (CTRL) mAb. Data are expressed as mean ± SD of percentage of Msi-1^{+} cells from five different experiments for α-Notch2/3 or hDLL4 and three different experiments for α-Notch1, *p<0.05; B) Representative analysis of Msi-1 expression in a primary sample: hDLL4 stimulation increased Msi-1 expression and this effect was completely blocked by α-Notch2/3. Gate are fixed on the isotype control and values indicate the percentage of Msi-1^{+} cells; C) Immunofluorescence analysis of MICOL-14^{tum} cells treated for 72h with α-Notch2/3, hDLL4, the combination of the two or with the corresponding control; nuclei were stained with TOPRO-3; magnification 40x; D) Western Blot analysis of Msi-1 and Numb protein with the control housekeeping tubulin. Protein lysates were obtained from MICOL-14^{tum} and primary cultures from liver metastases after treatment with α-Notch2/3, hDLL4, the combination of α-Notch2/3 and hDLL4 or the control BSA. The panels show one representative Western Blot out of three analyzed.

3.3 Effects of Notch2/3 blockade on spheroid-forming cells

As outlined above, Msi-1 is a well-recognized colon stem cell marker and one of the canonical features of cancer stem cells is their ability to form spheroids *in vitro*

under specific culture conditions. Based on these premises, we wondered whether Msi-1 reduction could lower the number of spheroid-forming cells. To test this hypothesis, we performed extreme limiting dilution assay (ELDA) with primary tumor cultures and MICOL-14^{tum} cells in the presence or absence of α-Notch2/3.

After four days, the frequency of spheroid-forming cells was significantly reduced by incubation with α-Notch2/3 antibody to 1/738 (upper 1/1046, lower 1/521), compared to the frequency recorded in the presence of a control antibody (1/239, upper 1/341 and lowe1/168) (Table 6). Similar results were obtained for MICOL-14^{tum} cells: the spheroid-forming cell frequency decreased from 1/142 (1/341- 1/168) to 1/428 (1/614-1/298) in the presence of α-Notch2/3 antibody (Table 6). These results indicate that attenuation of Msi-1 levels, associated with Notch2/3 blockade, could affect cancer stem cell features.

Number of cells/well	**Number of well plated**	**Number of well showing spheroids**			
		Human metastases		**MICOL14^{tum}**	
		CTRL	**α-Notch2/3**	**CTRL**	**α-Notch2/3**
2000	30	30	27	30	29
400	30	22	13	23	15
80	30	10	4	17	11
16	30	5	2	13	3
Frequency		1/239	1/738	1/142	1/428

Table 6. **α-Notch2/3 reduced spheroid forming ability**
Extreme limiting dilution analysis on MICOL-14^{tum} and primary samples incubated, at different concentrations as indicate in the table, for four days with α-Notch2/3 or CTRL antibody. Data were analyzed by a specific web-toll and the spheroids forming frequency represents a mean between the upper and lower results.

3.4 Msi-1 modulation is Notch3-dependent

These results seemed to indicate that blockade of either Notch2 or Notch3 activation perturbs Msi-1 levels in CRC cells. To determine which Notch paralog was mainly involved in this effect, we overexpressed either Notch3 or Notch2 intracellular domain (ICD) in MICOL-14^{tum} cells using retroviral vectors. We found that N3ICD overexpression induced a 3-fold increase in Msi-1 levels, together with

up-modulation of Notch3 and Hey2 levels (Fig. 23A). In contrast, expression of N2ICD increased Hey-2 mRNA levels but caused minimal variations of Msi-1 mRNA levels (Fig. 23B). These results indicate that hDLL4 up-regulates Msi-1 primarily by a Notch3-mediated mechanism.

To corroborate the hypothesis that Notch-3 regulates Msi-1, Msi-1 expression was investigated in tumor xenografts formed by MICOL-14^{tum} cells transduced by a lentiviral vector encoding a Notch3-specific shRNA (sh235); as reported in our previous study [89], these cells show a 60-80% decrease in Notch3 mRNA levels, compared to control shRNA cells. Immunohistochemical analysis demonstrated very low Msi-1 expression in tumors bearing low Notch3 levels (Fig. 23C), in line with the hypothesis that Notch3 has a key role in tuning Msi-1 levels in these cells.

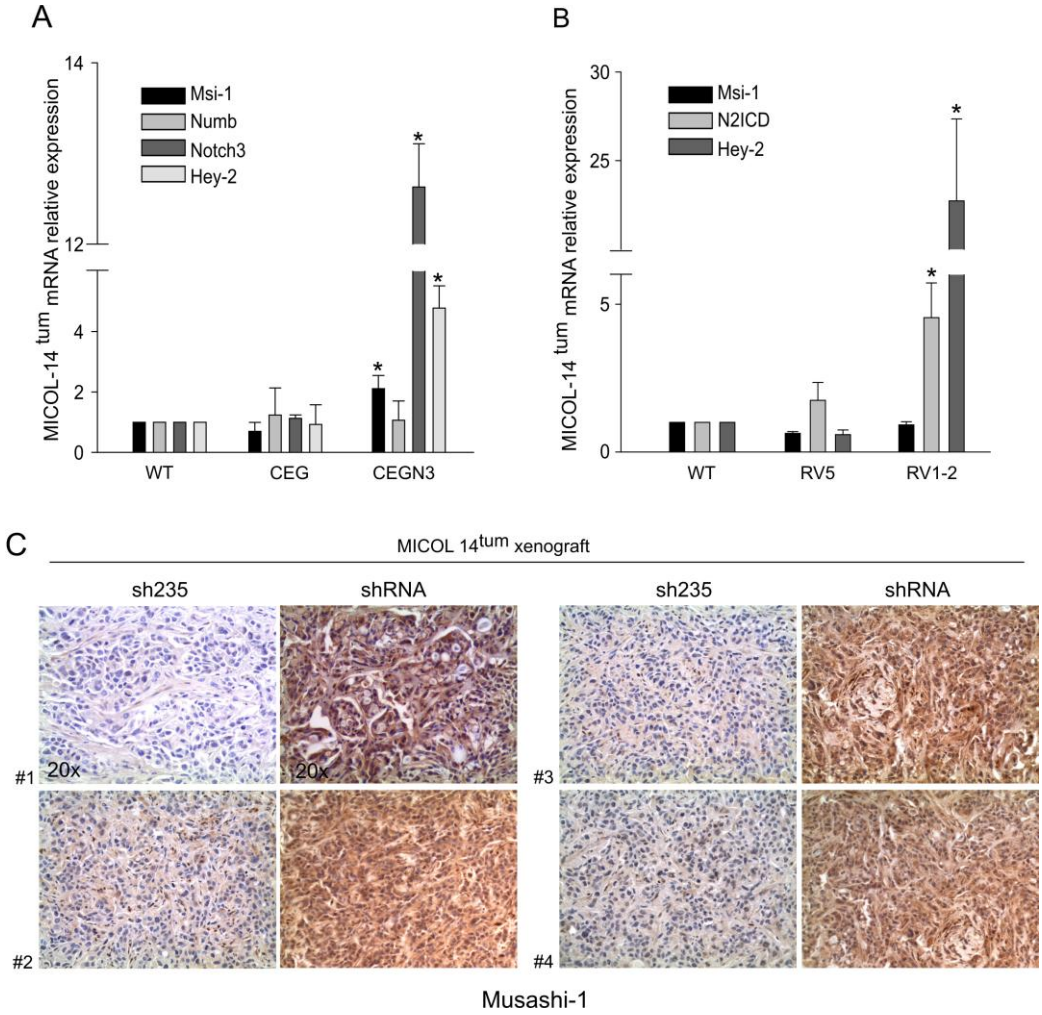

Figure 23. **Notch3 contributed to regulation of Msi-1 levels in CRC cells**
A) qRT-PCR after transfection of MICOLO-14^{tum} cells with Notch3 ICD (CEGN3) or the control vector (CEG). Msi-1, Notch3 as well as Hey-2, significantly increased while no alteration in Numb RNA levels were detected, comparing with control vector or no treated cells (wild type, WT). Data are expressed as mean ± SD of three different replicates; *p<0.05; B) qRT-PCR after transfection of MICOLO-14^{tum} cells with a vector encoding Notch2 ICD (RV1-2) or the empty vector (RV5). Only Notch2ICD and the target gene Hey-2 significantly increased. Overexpression of N2ICD did not affect Mis-1 levels comparing with control vector or no treated cells (wild type, WT). Data are expressed as mean ± SD of three different replicates; *p<0.05; C) Immonohistochemical analysis of Msi-1 expression on xenografts obtained by MICOL-14^{tum} cells transducted with a lentiviral vector (sh235) inducing a reduction of Notch3 mRNA levels or an empty vector (shRNA). Four different tumors were stained.

3.4 Effect of Notch3 modulation on Notch1 protein

Since Numb is a commonly recognized negative regulator of Notch1 [64], and Notch3 alteration induced modulation in Msi-1 protein that inhibits Numb, we analyzed whether also Notch1 could be influenced by Notch3 modulation. As expected, 72 h of stimulation with hDLL4 induced an increase of nuclear Notch1

activated form (N1ICD) in MICOL-14^{tum} cells (Fig. 24A) detected by immunofluorescence analysis. Furthermore, Western Blot analysis demonstrated that MICOL-14^{tum} cells transfected with a vector encoding for DLL4 showed an increase in N1ICD protein compared to the empty control vector (Fig. 24B); interestingly, the increase in N1ICD was also observed when MICOL-14^{tum} cells were transfected with a vector overexpressing Notch3 ICD (Fig. 24B), thus indicating a modulation in N1ICD induced by Notch3 alteration.

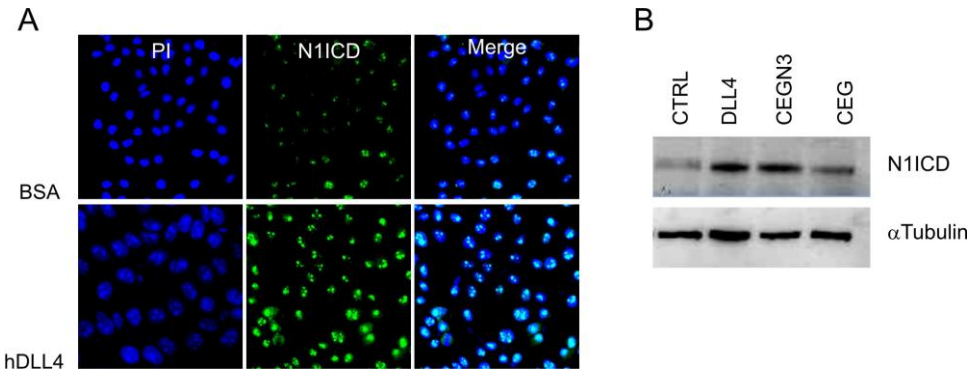

Figure 24. **Notch 3 overexpression increased Notch1 ICD**
A) Immunofluorescence of N1 activated domain (N1ICD) on MICOL-14^{tum} cells stimulated with hDLL4 for 72 h or BSA as control; hDLL4 increased the activation and transmigration of N1ICD into the nucleus (blu), one representative experiment is shown, magnification 40x; B) Western Blot analysis of N1ICD with the control housekeeping α-tubulin. Protein lysates were obtained from MICOL-14^{tum} cells transfected with a vector encoding DLL4, an empty control vector (CTRL), a vector overexpressing N3 (CEGN3) and the corresponding control (CEG). The panels show one representative Western blot.

DISCUSSION

Our study demonstrated that the ability to form spheroids in serum-free medium is not restricted to tumor and pre-cancerous samples [94, 95], but that epithelial cells isolated from normal colon biopsies and maintained in stem cell medium are also able to form spheroidal structures, morphologically comparable to those obtained from tumor colon samples. This ability was confined to a slowly cycling PKH^{pos} population, which survived *in vitro* in the absence of serum for up to 40 days. Indeed, after 6 weeks of culture the surviving population accounted for less than 5% of the input population; these cells, however, maintained a bright PKH26 staining. When transferred to a serum-containing medium, these cells underwent differentiation, as judged by the acquisition of adhesive properties, a different morphology, the loss of stemness markers, and the expression of typical differentiation markers such as CK20 and Muc-1/2.

The major achievement of our work is the *in vitro* culture and characterization of several discrete cell populations, some of which endowed with more prominent stem-like properties. In this regard, we focused our attention on two commonly recognized markers of colon stem cells, such as Msi-1 and Lgr5. Msi-1 is a RNA-binding protein that plays an essential role in regulating asymmetric cell division, by maintaining colon stem/progenitor cell proliferation and inhibiting the differentiation process [104]; Lgr5 is supposed to be a Wnt target gene, and its expression is lost as a consequence of the inhibition of the Wnt pathway [24]. Msi-1 and Lgr5 expression was evaluated in PKH^{high}, PKH^{low} and PKH^{neg} cell subsets, as representative of cell populations which underwent increasing cycles of replication. Cytofluorimetric analysis showed that Lgr5 expression was strictly confined to the PKH^{high} subset, and all $Lgr5^{+}$ cells also expressed Msi-1. On the contrary, even though Msi-1 was mainly expressed by PKH^{high} cells, not all $Msi\text{-}1^{+}$ cells also expressed Lgr5, and a small proportion of $Msi\text{-}1^{+}$ cells could also be found within PKH^{low} cells. In addition, while no co-expression of CK20 and Lgr5 could be documented, we identified a small subset of $Msi\text{-}1^{+}$ cells which also expressed the differentiation marker CK20. Thus, based on PKH26 staining and stemness/differentiation marker expression, a hierarchy of several distinct populations could be defined in our *in vitro* cultures: I) a $PKH^{high}/Lgr5^{+}/Msi\text{-}1^{+}/CK20^{-}$ subset, which likely reflects a relatively quiescent

stem-like population that did undergo minimal *in vitro* proliferation; II) a $PKH^{high}/Lgr5^{-}/Msi\text{-}1^{+}/CK20^{+}$ population that did undergo poor proliferation but expressed a differentiation marker; III) a $PKH^{low}/Lgr5^{-}/Msi\text{-}1^{+}/CK20^{-}$ subset, where part of the cells which underwent active replication still maintained the expression of a stemness marker; IV) a $PKH^{low}/Lgr5^{-}/Msi\text{-}1^{-}/CK20^{+}$ subset; and V) a $PKH^{neg}/Lgr5^{-}/Msi\text{-}1^{-}$ subset.

The location of the two small "transitional" subsets ($PKH^{high}/Lgr5^{-}/Msi\text{-}1^{+}/CK20^{+}$ cells and $PKH^{low}/Lgr5^{-}/Msi\text{-}1^{+}/CK20^{-}$ cells) within the developmental tree of colon epithelial cells is unclear. While both had lost the expression of one of the mostly recognized stemness markers, the former likely underwent poor replication (in view of its high PKH26 staining) and continued to express Msi-1 but in combination with a differentiation marker; the second subset ($PKH^{low}/Lgr5^{-}/Msi\text{-}1^{+}/CK20^{-}$) instead, while continuing to express some properties of immature cells, underwent proliferation without acquiring a differentiated phenotype. To our mind, the apparently contrasting properties of $PKH^{high}/Lgr5^{-}/Msi\text{-}1^{+}/CK20^{+}$ cells, which also express markers typical of goblet cells (Fig. 3), could reflect a sort of "committed" subset [105], where the relatively immature cells quickly acquire the expression of classical differentiation markers (such as CK20 and Muc-1/2), without showing a significant proliferative potential, as demonstrated by the maintenance of high levels of PKH26 staining. On the other hand, $PKH^{low}/Lgr5^{-}/Msi\text{-}1^{+}/CK20^{-}$ cells might represent the natural evolution of a rapidly cycling immature reservoir, which did not acquire differentiation markers but also did not completely loose self-maintaining properties. Within the limits of an analysis carried out in cells maintained *in vitro* in experimental, non-physiologic conditions, our observations might reconcile the debate on the relative quiescence of stem-like cells in the gastrointestinal tract [106], by showing that cells with differential expression of commonly recognized stemness markers may coexist and show different replicative potential.

Our phenotypic data are buttressed by the analysis of the transcriptomic profile of the above stemness/differentiation markers in PKH^{neg}, PKH^{low} and PKH^{high} cells, compared to that observed in cells obtained by the microdissection of distinct crypt portions (Fig. 4B). The cells isolated at the very bottom of the crypt expressed huge amounts of mRNA for both Msi-1 and Lgr5; on the other hand, differentiated cells at

the very top of the crypts only showed high levels of CK20, and no Msi-1/Lgr5 mRNA was detected. While these *ex vivo* results were not surprising, it is noteworthy that they fully mirrored the figures observed in the corresponding subsets expanded in culture (Fig. 4), further buttressing the notion that PKH^{high} cells do contain a cell population endowed with stem-like properties.

The analysis of putative stemness markers in normal colon epithelial cells seemed to identify Lgr5 and Msi-1 expression as a prominent feature of stem-like cells. Thus, we concentrate our attention on these particular markers, and addressed their relationship with other membrane receptor which have been claimed to participate in the tumorigenesis process, such as the members of the Notch family.

The presence of a slowly cycling cell population, expressing the stemness markers Msi-1 and Lgr5 and able to form spheroidal structure was thus analyzed in samples of CRC primary tumors and liver metastases. In tumor samples we could identify a PKH^{high} subset, persisting in *in vitro* culture for over five weeks, that mirrored the stem-like population found in normal samples. However, by analyzing the dye expression in the metastatic samples, we recorded the *in vitro* selection of a cell subset with intermediate PKH intensity: the PKH^{low} cells, while the PKH^{high} subset, also present in the total cell population, progressively declined over the culture period. Both PKH^{high} and PKH^{low} populations expressed Lgr5 and Msi-1, were able to form spheroids in PhEMA-treated plate, and to differentiate in the presence of serum loosing Msi-1 and Lgr5 expression while acquiring CK20 expression. These results seemed to indicate that in the metastatic samples the population endowed with stem-like features is not mainly confined to the non-cycling subset.

In the metastatic samples we focused our attention on Msi-1 expression. It is known that Msi-1 is a RNA-binding protein that acts to regulate Notch activation and migration to the nucleus, where it interacts with the DNA-binding protein CSL thus inducing transcription of specific target genes. Msi-1 protein, in fact, binds Numb mRNA thus inhibiting Numb-mediated degradation of Notch intracellular domain (ICD). Using a monoclonal antibody, we demonstrated that neutralization of Notch2/3 signaling affects Msi-1 levels in both the CRC cell line $MICOL\text{-}14^{tum}$ and primary human samples. We observed an increase in mRNA and protein Msi-1 levels after stimulation with a common ligand of the Notch pathway (hDLL4); in parallel

we observed a reduction of both Notch3 and Msi-1 levels after incubation with α-Notch2/3 mAb. No reduction was detected after incubation with α-Notch1. To understand whether Notch3 or Notch2 was involved, we performed qRT-PCR analysis of Msi-1 levels in MICOL-14^{tum} cells transfected with a vector overexpressing Notch2ICD or Notch3ICD: only N3ICD overexpression was associated with increase Msi-1 transcript levels. Moreover, 72 h of incubation with α-Notch 2/3 mAb increased Muc-1 protein, whereas stimulation with hDLL4 was associated with reduction of Muc-1. Since Muc-1 is a marker of colon epithelial cells differentiation, this result could indicate that neutralization of Notch2/3 promotes cell escape from stemness condition to undergo differentiation, as also supposed by the decrease in Msi-1 expression, the increase in Muc-1 levels and the reduction in the spheroid-forming cell frequency after Notch3 blockade.

Thus Notch3 appears to regulate Msi-1 expression at both protein and mRNA levels; as a consequence of this, we detected a modulation also in its target Numb and interestingly in Notch1ICD. It is known that Notch3 is a target of Notch1, but our results indicate for the first time a possible regulation of Notch1 by Notch3 probably through Msi-1, by a mechanism involving degradation of Numb mRNA and blocking its destabilizing effects on Notch1ICD. It has previously been demonstrated [107] that Numb and its four isoforms differentially inhibit the Notch ICD: using a luciferase-reporter Beres and colleagues determined the ability of each Numb isoform to inhibit significantly Notch1ICD; in contrast Notch3ICD was not inhibited by any of the Numb isoforms [107].

Based on the above findings and interpreting them with published data, we describe a novel feed-forward circuit of Msi-1, Numb, Notch3 and Notch1 regulation, schematized in Figure 25. Further work will be needed, to clarify how Msi-1 modulation occurs. Since Notch3 is a well-established transcriptional factor, we will firstly investigate the possible transcriptional regulation of Msi-1 by Notch3. We have already performed a bioinformatic analysis of the distribution of canonical and non-canonical CSL binding domains in Msi-1 promoter region and compared it with Hes1 and Hey2, well recognized Notch target genes. We observed a similar expression and distribution of the CSL-binding domains in the genes analyzed but will be necessary to validate this prediction by further experimental work.

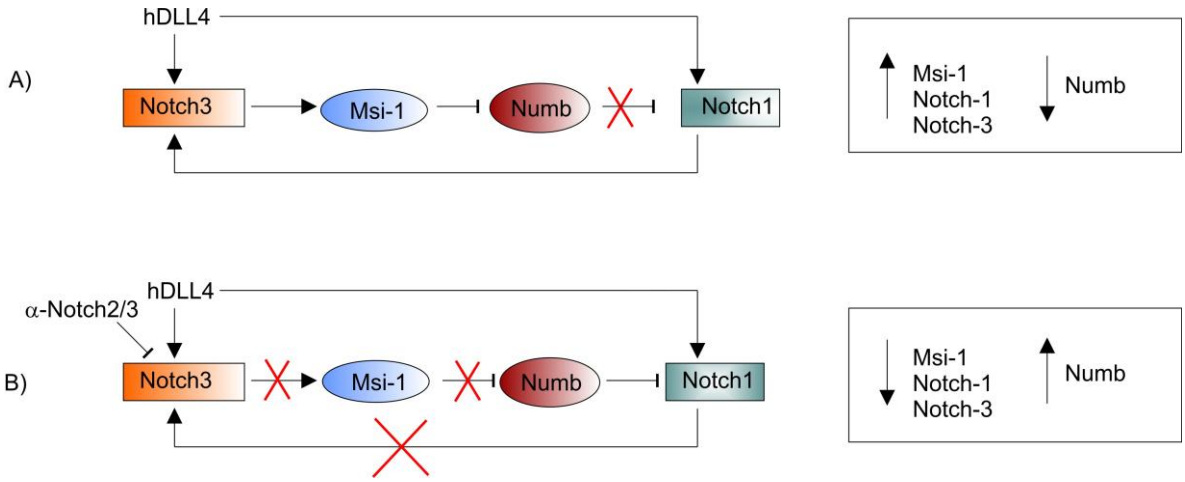

Figure 25. **Schematic representation of a novel feed-forward circuit of Msi-1 regulation.**
A) The Notch ligand DLL4 stimulates both Notch3 and Notch1; increase of Notch3 induces an increase of Msi-1 protein that binds Numb mRNA, thus repressing its inhibitory action effect Notch1. Activated Notch1 can migrate into the nucleus and induce the transcription of specific target genes such as Notch3; B) When Notch3 is inhibited, the reduced levels of Msi-1 don't inhibit Numb mRNA, thus limiting Notch signaling including further induction of Notch3 expression.

REFERENCES

1. Verfaillie CM, Pera MF, Lansdorp PM et al. Stem cells: hype and reality. *Hematology Am Soc Hematol Educ Program* (2002); 369–391

2. Weissman IL. Stem cells: units of development, units of regeneration, and units in evolution. *Cell* (2000); 100: 157–168

3. Li L and Bhatia R. Stem cells quiescence. Clin Cancer Res (2011); 17: 4936-4941

4. Barker N and Clevers. Leucine-Rich Repeat-Containing G-protein-coupled receptor as markers of adult stem cells. Gastroenterol (2010); 138: 1681-1696

5. Schofield R. The relationship between the spleen colony-forming cell and the haemopoietic stem cell. *Blood Cells* (1978); 4: 7–25

6. Li L, Xie T. Stem cell niche: structure and function. *Annu Rev Cell Dev Biol* (2005); 2:605–31

7. Spradling A, Drummond-Barbosa D, Kai T. Stem cells find their niche. *Nature* (2001); 414: *98*–104

8. Tumbar T, Guasch G, Greco V et al. Defining the epithelial stem cell niche in skin. *Science* (2004); 303: 359–63

9. He XC, Zhang J, Li L. Cellular and molecular regulation of hematopoietic and intestinal stem cell behavior. *Ann N Y Acad Sci* (2005); 1049: 28–38

10. Sato T, Stange DE, Ferrante M, et al. Long-term expansion of epithelial organoids from human colon, adenoma, adenocarcinoma, and Barrett's epithelium. *Gastroenterology* (2001); 141: 1762-72

11. Jung P, Sato T, Merlos-Suarez A et al. Isolation and in vitro expansion of human colonic stem cells. *Nature Med* (2011); 17: 1225-1227

12. Booth C and Potten C. Gut instinct: thoughts on intestinal epithelial stem cells. *J Clin Invest* (2000); 105: 1493-1499

13. Kumar V, Abbas AK, fausto N et al. Chapter 15. *In Robbin's Basic Pathology* (2007); 8th ed: 579-586

14. Potten CS, Kellett M, Roberts SA et al. Measurement of in vivo proliferation in human colorectal mucosa using bromodeoxyuridine. *Gut* (1992); 33: 71-78

15. Barker N, van de Wetering M and Clevers H. The intestinal stem cells.*Genes Dev* (2008);22: 1856-1864

16. Zeki S, Graham T and Wright N. Stem cells and their implications for colorectal cancer. *Gastroenterol Hepatol* (2011); 8: 90-100

17. Fujimoto K, Beauchamp RD, Whiteheal RH. Identification and isolation of candidate human colonic clonogenic cells based on cell surface integrin expression. *Gastroenterology* (2002); 123:1941–1948

18. Sophos NA, Vasiliou V. Aldehyde dehydrogenase gene superfamily: the 2002 update. *Chem Biol Interact* (2003);143–144:5–22.

19. Huang EH, Hynes MJ, Zhang T, Ginestier C et al. Aldehyde dehydrogenase 1 is a marker for normal and malignant human colonic stem cells (SC) and tracks SC overpopulation during colon tumorigenesis. *Cancer research* (2009); 69: 3382

20. Khalek FJA, Gallicano GI and Mishra L. Colon cancer stem cells. *Gastrointest Cancer Res Supll* (2010); 1: 16-23

21. Nishimura S, Wakabayashi N, Toyoda K et al Expression of Musashi-1 in Human Normal colon crypt cells. *Digestive diseases and sciences* (2003); 48: 1523-1529

22. May R, Riehl TE, Hunt C et al. Identification of a novel putative gastrointestinal stem cell and adenoma stem cell marker, doublecortin and CaM kinase-like-1, following radiation injury and in adenomatous polyposis coli/multiple intestinal neoplasia mice. *Stem Cells* (2008); 26: 630–637

23. Sangiorgi E and Capecchi MR. Bmi1 is expressed in vivo in intestinal stem cells. *Nature Genetics* (2008); 40: 915-920

24. Barker N, Van Es JH, Kuipers J et al. Identification of stem cells in small intestine and colon by marker gene Lgr5. *Nature* (2007): 449:1003-1007

25. Barker N, Ridgway RA, Van ES JH et al. Crypt stem cells as the cells-of-origin of ntestinal cancer. *Nature Letters* (2009); 457: 608-612.

26. Nakamura M, Okano H, Blendy Aj and Montell C. Musashi, a neural RNA-binding protein required for Drosophila adult external sensory organ development. *Neuron* (1994); 13:67-81

27. Sugiyama-Nakagiri Y, Akiyama M, Shibata A et al. Expression of RNA-binding Musashi in hair follicle development and hair cycle progression. *Am J Pathol* (2006); 168: 80-92

28. Kayahara T, Sawada M, Takaishi S et al. Candidate markers for stem and early progenitor cells, Musashi-1 and Hes-, are expressed in crypt base columnar cells of mouse small intestine. *FEBS Lett* (3003); 535: 131-135

29. Clarke RB, Spence K, Anderson E et al. A putative human breast stem cell population is enriched for sferoid receptor-positive cells. *Dev Biol* (2005); 277: 443-456

30. Okano H, Kawahara H, Toriya M et al. Function of RNA-binding protein Musashi-1 in stem cells. *Exp Cell Res* (2005); 306: 349-356

31. Imai T, Tokunaga A, Yoshida T et al. The neural RNA-binding protein Musashi1 translationally regulates mammalian numb gene expression by interacting with its mRNA. *Mol Cell Biol* (2001); 21: 3888-3900

32. Battelli C, Nikopopulos GN, Mitchell JG et al. The RNA-binding protein Musashi-1 regulates neural development through the translational repression of p21WAF-1. *Mol Cell Neurosci* (2006); 31: 85-96

33. Horisawa K, Imai T, Okano H et al. 3'-Untranslated region of dublecortin mRNA is a binding target of the Musashi1 RNA-binding protein. *FEBS Lett* (2009); 583: 2429-2434

34. Jordan CT, Guzman ML and Noble M. Cancer Stem cells. *New England J Medicine* (2006); 355: 1253-1261

35. Moserle L, Ghisi M, Amadori A et al. Side population and cancer stem cells: therapeutic implications. *Cancer Lett* (2010); 288:1-9.

36. Charafe-Jauffret E, Ginestier C, Iovino F et al. Breast cancer cell lines contain functional cancer stem cells with metastatic capacity and a distinct molecular signature. *Cancer Res* (2009); 69: 1302-1313.

37. Fan X, Matsui W, Khaki L et al. Notch pathway inhibition depletes stem-like cells and blocks engraftment in embryonal brain tumors. *Cancer Res* (2006); 66: 7445-7452

38. Cicalese A, Bonizzi G, Pasi CE, et al. The tumor suppressor p53 regulates polarity of self-renewing divisions in mammary stem cells. *Cell* (2009); 138: 1083-1095.

39. Todaro M, Alea MP, Di Stefano AB et al. Colon cancer stem cells dictate tumor growth and resist cell death by production of interleukin-4. *Cell Stem Cell* (2007); 1: 389-40

40. Hirschmann-Jax C, Foster AE, Wulf GG, et al. A distinct "side population" of cells with high drug efflux capacity in human tumor cells. *Proc Natl Acad Sci U S A* (2004); 10: 14228-14233.

41. Moitra K, Lou H et Dean M. Multidrug efflux pumps and cancer stem cells: insights into multidrug resistance and therapeutic development. *Clin Pharmacol Ther* (2011); 89: 491-502

42. Ricci-Vitiani L, Lombardi DG, Pilozzi E et al. Identification and expansion of colon-cancer-initiating cells. *Nature* (2007); 445:111-115

43. O'Brien CA, Pollett A, Gallinger S et al. A human colon cancer cell capable of initiating tumor growth in immunodeficient mice. *Nature* (2007); 445:106-110

44. Shmelkov SV, Butler JM, Hooper AT, et al. CD133 expression is not restricted to stem cells, and both $CD133^+$ and $CD133^-$ metastatic colon cancer cells initiate tumors. *J Clin Invest* (2008); 118: 2111–2120.

45. Dalerba P, Dylla SJ, Park IK et al. Phenotypic characterization of human colon cancer stem cells. *Proc Natl Acad Sci USA* (2007); 104: 10158-10163

46. Todaro M, Perez A, Scopelliti JP et al. IL-4 mediated drug resistance in colon cancer stem cells. *Cell Cycle* (2008); 7: 309-313

47. Vermuelen L, Todaro M, de Sousa Mello et al. Single-cell cloning of colon cancer stem cells reveals a multi-lineage differentiation capacity. *Proc Natl Acad Sci USA* (2008); 105: 13427-13432

48. Huang EH, Hynes MJ, Zhang T et al. Aldehyde dehydrogenase 1 is a marker for normal and malignant human colonic stem cells (SC) and tracks SC overpopulation during colon tumorigenesis. *Cancer Res* (2009); 69: 3382-3389

49. Muraro MG, Mele V, Daster S et al. $CD133^+$,$CD166^+CD44^+$, and $CD24^+CD44^+$ phenotypes fail to reliably identify cell population with cancer stem functional features in established human colorectal cancer cell line. *Stem Cell Transl Med* (2012); 1: 592-603

50. Jemal A, Siegel R Xu J et al. Cancer statistics, 2010. *Cancer J Clin* (2011); 6: 133-134

51. Frank SA. Dynamics of cancer: incidence, inheritance and evolution. Princeton (NJ): princeton University press (2007); Chapter 3

52. Ionov Y, Peinado MA, Malkhosyan S et al. Ubiquitous somatic mutations in simple repeated sequences reveal a new mechanism for colon carcinogenesis. *Nature* (1993); 363: 558-561

53. Rizk P and Barker N. Gut stem cells in tissue renewal and disease: methods, markers and myths. *WIREs Syst Biol Med* (2012); 4: 475-496

54. Liotta LA, Kohn EC. Cancer's deadly signature. *Nat Genet* (2003); 33: 10-11

55. Kessenbrock K, Plaks V and Werb Z. Matrix metalloproteinases: regulators of the tumor microenvironment. *Cell* (2010); 141: 52-67

56. Thompson EW and Haviv I. The social aspect of EMT-MET plasticity. *Nature Med* (2011); 17: 1048-1049

57. Wharton KA, Johansen KM, Xu t et al. Nucleotide sequence from the neurogenic locus notch implies a gene product that share homology with proteins containing EGF-like repeats. *Cell* (1985); 43: 567-581

58. Fiuza UM and Arias AM. Cell and molecular biology of Notch. *J Endocrinol* (2007); 194: 459-474

59. Kopan R. Notch: a membrane-bound transcription factor. *J Cell Sci* (2002); 115: 1095-1097

60. D'Souza B, Miyamoto A and Weinmaster G. The many facets of Notch ligands. *Oncogene* (2008); 27: 5148-5167

61. Thurston G, Noguera-Troise I and Yancopoulos GD. The Delta paradox: DLL4 blockade leads to more tumour vessels but less tumour growth. *Nat Rev Cancer* (2007); 7: 327-331

62. Wu L and Griffin JD. Modulation of Notch signaling by mastermind-like (MAML) transcriptional co-activators and their involvement in tumorigenesis. *Semin Cancer Biol* (2004); 14: 348-356

63. Leon KG and Karsan A. Recent insights into the role of Notch signaling in tumorigenesis. *Blood* (2006);107: 2223-2233

64. Glazer RI, Wang XY, Yuan H et al. Musashi-1 a stem cell marker no longer in search of a function. *Cell Cycle* (2008); 7: 2635-2639

65. Sander GR and Powell BC. Expression of notch receptors and ligands in the adult gut. *J Histochem Cytochem* (2004); 52: 509-516

66. van Es JH, van Gijn ME, Riccio O et al. Notch/gamma-secretase inhibition turns proliferative cells in intestinal crypts and adenomas into goblet. *Nature* (2005); 435: 959-963

67. Fre S, Huyghe M, Mourikis P et al. Notch signals control the fate of immature progenitor cells in the intestine. *Nature* (2005); 435: 964-968

68. Riccio O, van Gijn ME, Bezdek AC et al. Loss of intestinal crypt progenitor cells owing to inactivation of both Notch1 and Notch2 is accompanied by derepression of CDK inhibitors p27Kip1 and p57Kip2. *EMBO Rep* (2008); 9: 377-383

69. Jensen J, Pedersen EE, Galante P et al. Control of endodermal endocrine development by Hes-1. *Nat Genet* (2000); 24: 36-44

70. Suzuki K, Fukui H, Kayahara T et al. Hes1-deficien mice show precious differentiation of Paneth cells in the small intestine. *Biochem Biophys Res Commun* (2005);328: 348-352

71. Jenny M, Uhl C, Roche C et al. Neurogenin3 is differentially required for endocrine cell fate specification in the intestinal and gastric epithelum *EMBO J* (2002); 21: 6338-6347

72. Ng AY, Waring P, Ristevski S et al. Inactivation of the transcription factor Elf3 in mice results in dysmorphogenesis and altered differentiation of intestinal epithelium *Gastroenterology* (2002); 122:1455-1466

73. van der Flier LG and Clevers H. Stem cells, self-renewal, and differentiation in the intestinal epithelium. *Annu Rev Physiol* (2009); 71: 241-260

74. Wang J, Wakeman TP, Lathia JD et al. Notch promotes radioresistance of glioma stem cells. *Stem Cells* (2010); *28*:17-28

75. Farnie G and Clarke RB. Mammary stem cells and breast cancer-role of Notch signalling. *Stem Cell Rev* (2007); 3: 169-175

76. Katoh, M. Notch signaling in gastrointestinal tract (review). *Int J Oncol* (2007); 30: 247-251

77. Ji Q, Hao X, Zhang M et al. MicroRNA miR-34 inhibits human pancreatic cancer tumor-initiating cells. *PLoS One* (2009); 4: e6816

78. Zhang T, Otevrel T, Gao Z et al. Evidence that APC regulates survivin expression: a possible mechanism contributing to the stem cell origin of colon cancer. *Cancer Res* (2001); 61: 8664-8667

79. Ulasov IV, Nandi S, Dey M et al. Inhibition of Sonic hedgehog and Notch pathways enhances sensitivity of CD133(+) glioma stem cells to temozolomide therapy. *Mol Med* (2011); 17: 103-112

80. Fan X, Matsui W, Khaki L et al. Notch pathway inhibition depletes stem-like cells and blocks engraftment in embryonal brain tumors. *Cancer Res* (2006); 66: 7445-7452

81. Hoey T, Yen WC, Axelrod F et al. DLL4 blockade inhibits tumor growth and reduces tumor-initiating cell frequency. *Cell Stem Cell* (2009); 5: 168-177

82. Dontu G, Jackson KW, McNicholas E et al. Role of Notch signaling in cell-fate determination of human mammary stem/progenitor cells. *Breast Cancer Res* (2004); 6: R605-615

83. Serafin V, Persano L, Moserle L et al. Notch3 signaling promotes tumor growth in colorectal cancer. *J Pathol* (2011); 224: 448-460

84. Todaro M, Alea MP, Di Stefano AB et al. Colon cancer stem cells dictate tumor growth and resist cell death by production of interleukin-4. *Cell Stem Cell* (2007); 1: 389-402.

85. Dalerba P, Guiducci C, Poliani PL et al. Reconstitution of human telomerase reverse transcriptase expression rescues colorectal carcinoma cells from in vitro senescence: evidence against immortality as a constitutive trait of tumor cells. *Caner Res* (2005); 65: 2321-2329

86. Indraccolo S, Minuzzo S, Masiero M et al. Cross-talk between tumor and endothelial cells involving the Notch3-Dll4 interaction marks escape from tumor dormancy. *Cancer Res* (2009); 69: 1314-1323

87. Cicalese A, Bonizzi G, Pasi CE et al.The tumor suppressor p53 regulates polarity of self-renewing divisions in mammary stem cells. *Cell* (2009); 138: 1083-1095

88. Moserle L, Ghisi M, Amadori A and Indraccolo S. Side population and cancer stem cells: therapeutic implication. *Cancer Lett* (2010); 288: 1-9.

89. Weng AP, Ferrando AA, Lee W et al. Activating mutations of NOTCH1 in human T cell acute lymphoblastic leukemia. *Science* (2004); 306: 269-271

90. Ghisi M, Corradin A, Basso K et al. Modulation of microRNA expression in human T-cell development: targeting of NOTCH3 by miR-150. *Blood* (2011); 117: 7053-7062

91. Williams CK, Li JL, Murga M, Harris AL et al. Up-regulation of Notch ligand Delta-like 4 inhibits VEGF-induced endothelial cell function. *Blood* (2006); 107: 931-939

92. Indraccolo S, Habeler W, Tisato V, et al. Gene transfer in ovarian cancer cells: a comparison between retroviral and lentiviral vectors. *Cancer Res* (2002*); 62*: *6099*–107

93. Lanzkron S, Collector M, Sharkis SJ. Hematopoietic stem cell tracking in vivo: a comparison of short-term and long-term repopulating cells. *Blood* (1999); 93: 1916-1921.

94. Visvader JE, Lindeman GJ. Cancer stem cells in solid tumors: accumulating evidence and unresolving questions. *Nature review* (2008); 8: 755-767.

95. Morrison JB, Schmidt CW, Lakhani SR et al. Breast cancer stem cells: implications for therapy of breast cancer. *Breast Cancer Res* (2008); 10: 210.

96. Sato T, Vries RG, Snippert HJ et al. Single Lgr5 stem cells build crypt-villus structures in vitro without a mesenchymal niche. *Nature* (2009); 459: 262-265.

97. Takeda K, Kinoshita I, Shimizu Y et al. Expression of LGR5, an intestinal stem cell marker, during each stage of colorectal tumorigenesis. *Anticancer Res* (2011); 31: 260-270

98. Humphries A, Wright N. Colonic crypt organization and tumorigenesis. *Nat Rev Cancer* (2008); 8: 415-424

99. Roig AI, Eskiocak U, Hight SK et al. Immortalized epithelial cells derived from human colon biopsies express stem cell markers and differentiation in vitro. *Gastroenterology* (2010); 138: 1012-1021.

100. Schulenburg A, Cech P, Herbacek I et al. CD44-positive colorectal adenoma cells express the potential stem cells markers musashi antigen (msi1) and ephrin B2 receptor (EphB2). J Pathol (2007); 213: 152-160

101. Huang EH, Hynes MJ, Zhang T et al. Aldehyde dehydrogenase 1 is a marker for normal and malignant human colonic stem cells (SC) and tracks SC overpopulation during colon tumorigenesis. *Cancer Res* (2009); 69: 3382-3389

102. Dalerba P, Kalisky T, Sahoo D et al. Single-cell dissection of transcriptional heterogeneity in human colon tumors. *Nature Biothecnol* (2011); 29: 1120-1127.

103. Gopalakrishnan N, Jayanthi V and Devaraj H. c-kit and Musashi-1 expression in colorectal carcinoma and its association with etiological factora. *Oncol Gastroenterol Hepatol Reports* (2012); 1:25-32

104. MacNicol A, Wilczynska A, MacNicol M. Function and regulation of the mammalian Musashi mRNA translational regulator. *Biochem Soc Trans* (2008); 36: 528-530.

105. Dangles-Marie V, Validire P, Richon S et al. Isolation and characterization of spontaneous spheroid aggregates within human colon carcinomas. *J Clin Oncol* (2007); 25: 14515

106. Shaker A, Rubin DC. Intestinal stem cells and epithelial-mesenchymal interactions in the crypt and stem cell niche. *Transl Res* (2010); 156: 180-187.

107. Beres BJ, George R, Laugher E et al. Numb regulates Notch1, but not Notch3, during myogenesis. *Mech Dev* (2011); 128: 247-257